Journal of Energy Storage 50 (2022) 104218

Contents lists available at ScienceDirect

Journal of Energy Storage

journal homepage: www.elsevier.com/locate/est

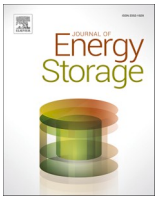

Research Papers

In-situ instrumentation of cells and power line communication data acquisition towards smart cell development

Timothy A. Vincent *, Begum Gulsoy, Jonathan E.H. Sansom, James Marco

Cell Instrumentation Team, WMG, University of Warwick, Coventry, West Midlands CV4 7AL, United Kingdom

ARTICLE INFO

Keywords:
Lithium-ion battery experimentation
Cell instrumentation
Power line communication (PLC)
Cell temperature sensing
Cell cycling
Battery performance characterisation

ABSTRACT

The internal core temperature of cells is required to create accurate cell models and understand cell performance within a module. Pack cooling concepts often trade off temperature uniformity, vs cost/weight and complexity. Poor thermal management systems can lead to accelerated cell degradation, and unbalanced ageing. To provide core temperature an internal array of 7 thermistors was constructed; these in conjunction with cell current, via bus bar mounted sensors, and voltage sensor measurements, we have developed instrumented cells. These cells are also equipped with power line communication (PLC) circuitry, forming smart cells. We report upon data from these miniature sensors during cell cycling, demonstrating successful operation of the PLC system (zero errors compared to a reference wired connection) during typical cell cycling (C/2 discharge, C/3 charge) and the application of automotive drive cycle, providing a transient current test profile. Temperature variation within the cell of approximately 1.2 °C gradients, and variation of >2.8 °C during just 30 min of 2C discharging demonstrate the need for internal sensing and monitoring throughout the lifetime of a cell. Our cycling experimental data, along with thorough cell performance tracking, where typically <0.5% degradation was found following instrumentation process, demonstrate the success of our novel prototype smart cells.

1. Introduction

Electrification of the transport sector is seen as the vital pathway to reducing carbon dioxide (CO_2) emissions [1]. In the United Kingdom, this sector currently accounts for 33% of CO_2 emissions [2], however, the current generation of lithium-ion (li-ion) battery packs typically deployed in domestic electric vehicles (EVs) are not feasible for use in commercial vehicles. Notably, heavy duty trucks, due to lack and range and extended downtime at required to undertake a full-charge [3,4], nor the aerospace industry, where strict safety regulations, insufficient energy density, insufficient durability and life expectancy concerns [5]. Increasing energy density, reducing charging times and improving motor efficiency are essential to continue electrification in the automotive and aerospace industries [6]. Equally, we propose our advances in smart cell research will be applicable to other sectors, such as energy storage and second life applications.

The cells developed in this work will help address the challenges in developing battery packs and associated cooling systems. Traditionally, during pack development when sensors are placed external to the cell, they fail to capture the peak core temperatures experienced by the cell, rather capturing only a mixture of the surface and environmental temperatures. In this work, by instrumenting the cells internally, and developing a viable method of acquiring sensor data, we demonstrate the benefits of understanding core temperature and present the opportunity to better instrument cells (our data acquisition system is compatible with, e.g. pressure, gas or other digital and analogue sensors). Our novel work includes the development and experimentation with thermistor sensor arrays, designed to be robust to the harsh cell environment, as well as sufficiently compact, to present no degradation to cell performance during our testing.

In the automotive market, EV sales have deviated from the 2020 reduction in overall vehicle sales, where a 143% growth in sales is reported, compared to an overall decrease of 24% in new car sales [7]. In 2020 almost 1.4 million battery and plug in hybrid EVs were sold in Europe. Current global regulations dictate EV passengers must be allowed a 5 min period to evacuate the vehicle in the event of battery failure. Specifically, this is the period required before smoke egress into the cabin, or between cell failure and complete pack failure [8]. Despite these requirements, EV fires are regularly captured in news articles, perhaps due to the excitement of these emerging technologies, although

* Corresponding author.
E-mail address: T.A.Vincent@warwick.ac.uk (T.A. Vincent).

https://doi.org/10.1016/j.est.2022.104218
Received 19 November 2021; Received in revised form 19 January 2022; Accepted 11 February 2022
Available online 26 February 2022

their occurrence is comparable or less than internal combustion engine (ICE) vehicles. For example, in has been reported hazardous EV failures occurred in around 0.9 to 1.2 cases per 10,000 EVs in China, compared to approximately 1.06 for ICE counterparts. In the United States, 7.3 cases per 10,000 ICE has been reported [9]. Consumer concern is noted to propagate from the risk of spontaneous fires, or becoming trapped in a vehicle, where re-ignition of EV fires is sometimes reported [9,10].

EVs are equipped with battery management systems (BMS) which, amongst other tasks, monitor and thermally manage the battery pack. In current EVs, these systems are typically limited to less than 20 sensors, perhaps for a pack containing hundreds of cells electrically connected in both series and parallel [11–13]. Increasing the instrumentation inside a battery pack is essential to enable the BMS to rapidly respond to individual cell issues [14]. It has been reported that a lack of sensors, and lack of redundancy, has prevented the early detection of battery fires and led to the failure of battery packs [5,15,16]. These incidents are not limited to electric cars, but extend to electric buses, where faulty sensors and no backup sensors have been found to be accountable for vehicle fire [16]. Such hazardous events have also been reported within the auxiliary battery packs within aircraft. In the aerospace industry, it is vital to understand the source of the failure, however current insufficient monitoring does not allow the specific cell, which triggered the event, to be found [17]. It is proposed, in the aerospace industry, rigorous monitoring, and perhaps refined cell control systems are needed. Furthermore, it is estimated a 15% increase in vehicle range could be achieved through individual cell control [18].

In this work we uniquely instrument our cells with a thermistor-based sensor array, that interfaces to a data logging BMS, via a power line communication (PLC) network. Here we detail our cell instrumentation procedure, as well as reporting upon our rigorous preliminary experimentation to ensure the sensors are resilient to the harsh internal cell environment. To the authors' knowledge instrumented cells equipped with powerline modems have not previously been studied. Through our novel instrumentation and communication network, we demonstrate a scalable method of instrumenting cells *in-situ*, where the number of nodes (i.e. cells) can be increased without introducing additional bulky wiring, as previously reported the literature and discussed in Section 2.2. This will enable cells to be equipped with thorough instrumentation – here temperature with high spatial resolution, current and voltage data for each individual cell are tested. The cells are without bulky cabling and then viable to be installed on commercial bus-bars, for example in module configurations, and be tested without needing extra communication/interface wiring. Traditionally, the industry standard sensor communication cabling means cells need to be physically located further apart to allow space for cable runs. By removing this additional cabling, this will help develop modules for use in future applications (e.g. EVs or aerospace), leading to deployment of instrumented cells. We propose that throughout their lifetime, instrumented cells with PLC will be able to record and log key data points, enabling better understanding of their state of health, and therefore easier categorising for deployment in second life applications. Instrumented cells are key to optimise energy storage, and monitor cell performance from formation/manufacture to end of life.

1.1. Li-ion cells

Compared to previous battery technologies, li-ion cells offer superior energy density, it is reported up to 250 Wh/kg [19] per cell, compared to a maximum of approximately 80 and 120 Wh/kg for NiCd and NiMH cells, respectively [20]. To meet the energy density requirements, while maintaining or improving safety systems, particularly for larger vehicles (i.e. larger road vehicles, or aircraft), improved instrumentation is required in the pack. This must be achieved while also minimising the physical volume impact and integration complexity, in terms of wiring, reliability, BMS processing load. Current pack designs decrease energy density (nearly 170 Wh/kg [19]) due to the integration of bulky electrical and cooling systems. It is proposed by better understanding of cell operation, pack design can be improved and optimised, thus enabling a greater energy density to be achieved. It is predicted an energy density of 400 Wh/kg per cell is required to allow electric aircraft to be feasible replacements for combustion equivalents. For example, several flights per day are needed, with at least a 500 mile range [19] and timely service intervals. It is noted current li-ion cells lifetime in order of 1000 cycles [5]). Our sensor technology is designed to be adaptable regardless of battery technology. Solid-state cells with lithium metal anodes have been suggested to advance current li-ion chemistries (greater than 500 Wh/kg, with improved safety and recyclability) and prototype cells could be ready for testing in EVs in as little as the next 10 years [21]. We aim to make our sensors and networking systems capable of integration within a range of cell formats, sizes and chemistries.

We propose, firstly, improved instrumentation (equipping cells with a greater number of sensors, offering higher resolution and accuracy) is required for future battery packs (EV, aerospace markets), to enable the BMS to optimise utilization of the pack (extending pack life, preventing thermal events, providing accurate measurement of cell state of health, SoH). Secondly, an improved understanding of cell performance is required prior to pack deployment, during the development of packs (cell format, arrangements etc.) and associated temperature management systems (air or liquid cooled, location of cooling/heating elements etc.).

Smart cells are a key component towards better understanding of a cell, from formation to end-of-life. During pack design, an understanding of cell operation and interaction between cells are vital. We envisage smart cells will help with pack development, and will be important in safety-critical applications, such as in the electrifying the aerospace industry. In such applications, component cost and development effort are secondary to the need to fully understand system operation, both during fabrication and deployment. In other applications, smart cells can be tailored in terms of component cost, and volume of data collected. During development, high precision and spatial resolution data will be required within a battery pack. In final applications requiring lower-cost solutions, smart cells could be distributed infrequently around a pack, and provide reference datapoints for the models incorporated within the BMS.

In our previous work [22] we have discussed instrumenting cells with voltage, current and external temperature sensors and networking these cells together with a master data logger to form a smart module – here defined as instrumented cells with integrated electronic communication circuitry. In this work we extend this concept, uniquely demonstrating our prototype smart cells, each equipped with an internal temperature sensing array, and a PLC modem to communicate with a master controller. A temperature sensing array has been inserted internally into the core of 21700 format cylindrical cells (7x sensors, providing 10 mm spatial resolution) to investigate core temperature variation during typical cycling. In this work, cells are cycled via charging and discharging, according to manufacturer specification, and later further tested with a transient drive cycle. The cells are tested individually (capacity and impedance checks), to verify successful instrumentation. They are then arranged in a small module (2 series, 2 parallel, 2S2P) to assess performance during cycling and demonstrate the PLC network (consisting of 4 slaves and 1 master node). In this paper we focus on the instrumented cells – the operation of the PLC network, with one node per cell, has been detailed in a dedicated article [23].

This paper is structured as follows: firstly, we discuss previous works in the literature regarding cell instrumentation and integration with communication circuitry; we then introduce our experimental setup and explain our component selection process. In the results and discussion section we highlight a subset of the overall findings from our smart cell experimentation. Finally, we conclude our smart cell work and briefly summarise our ongoing and future work.

2. Cell instrumentation background

2.1. Temperature monitoring and cooling system design

Thermocouple sensors are typically used in EV battery packs to monitor temperature at specific locations within the pack [12]. Each sensor requires a cold junction; thus, each sensor is normally connected to a reference unit, preventing multiple thermocouple connections in series. In a traditional setup, this entails each additional sensor requires further wiring, leading to a trade-off for pack designers between instrumentation resolution and pack cost/complexity [14].

Temperature gradients inside li-ion cells cause inhomogeneous current density distributions within the jelly roll of the cell, leading to local ageing and subsequently influencing global ageing [24,25]. The distribution of these temperature gradients is not yet fully understood. Manufacturing defects and tolerances can create unpredictable temperature gradients. These defects sometimes exacerbate during the life of the cell, thus making it challenging to detect faults during manufacture [26]. These local defects can eventually grow significantly, and lead to cell failure and possible thermal runaway [27]. Cooling systems should be designed to maintain a uniform temperature profile throughout the cell. These systems however, influence the energy density of the pack and therefore vehicle cost, range and driving performance capability [28]. Energy density is critical to enable electrification of the transport and aerospace industries, as well as matching capability (range or endurance, weight, size) of ICE vehicles [6,29]. Thus BMS size and weight, including that of associated wiring, circuitry and integrated systems, must be minimised. This is a key driver for automotive manufacturers [30]. Cell instrumentation is critical to develop accurate models during cell modelling or cooling system development. However, we propose a level of cell instrumentation would be beneficial during operation, to quickly identify hot spot formation and monitor the ageing of individual cells.

Air cooling has been implemented in many EVs on the market (e.g. Nissan Leaf, Toyota Prius, Volkswagen ID.3 [31]); the low thermal conductivity of air limits its effectiveness in environments with higher ambient temperatures. Liquid cooling offers superior heat capacity and thermal conductivity, although its effectiveness is still governed by system design [31]. The temperature profiles of 18,650 cells cooled by radial and tab techniques have been studied [32]. Radial cooling requires a more complex system, i.e., greater access needed to the surface of the cells. However it has been reported it can maintain a temperature gradient of <5 °C cell; in the scenario of a drive profile [32]. In this case, heat generation was assumed to be less than 1.1 W, with around a 2C charge rate. Tab cooling was noted to be able to maintain similar performance. However, this type of cooling moved the hot spot of the cell from the core to the un-cooled tab. Non-uniform cooling of cells can increase ageing effects and therefore degrade the cell. A study of 2C discharge by Robinson et al. found a large temperature gradient of ~10 °C with an 18650 format cell, where the higher temperatures were observed towards the positive end of the cell [33] (an external measurement technique was implemented, avoiding the use of internally instrumented cells). A poorly designed cooling system can worsen the condition and quickly degrade the overall capacity of the pack [34–36].

In many applications, such as laptop computers, small vehicles and hand tools/equipment [37], cylindrical format cells are preferred compared to pouch or prismatic for their maturity, potentially improved life cycle and improved consistency. Their shape reduces the accessibility of surfaces for cooling, thereby increasing the difficulty of practically implementing an effective cooling system [28]. Lai et al. discuss the design of a cooling system for cylindrical cells, and investigate the necessary cooling structure around each cell, needed to maintain a functional temperature when the cells were charged at 5C [28]. The importance of optimising the cooling system design is expressed, and visualised by the formation of hot areas within the cell, when coverage of the cooling system is sub-optimum. The study demonstrates the need for careful design of cooling structures, but also highlights the reliance on simulated data, despite the acknowledged error to experimental data (>1 °K in cases).

Despite the challenges cooling cylindrical cells, due to their low core-to-surface ratio, such a mature technology is still preferred for pack development in many applications. One advantage of cylindrical cells is noted, where it is estimated a pack based on pouch cells requires a volume three times greater (considering the overall pack structure) to achieve similar energy capacity, as well as protection against the vulnerability to puncturing (soft material) [20]. In this work we focus on 21700 format cylindrical cells, although our techniques could be adapted to prismatic or perhaps pouch cells as required.

2.2. Miniature sensors

In general, cylindrical cells require greater spatial resolution to locate hot spots compared to pouch cell counterparts (considering both of equal energy capacity). Compared to a pouch cell layout, the circular wrapping of the jelly roll and greater layer density leads to poorer thermal conductivity properties in the radial plane of cylindrical cells. This phenomenon has previously being explored, via the placement of miniature thermocouples inside an 18,650 cell (between layers of the jelly roll) [38]. In the through plane direction between the separator and electrodes, low energy density of around 1 W m^{-1} K^{-1} was reported. This is supported by studies cycling cells, and demonstrating up to 5 °C variation between surface and core temperature during standard operation when the cell is operated within its manufacturer's defined specification [14, 39–41]. It is reported in the order of around only 3 °C is found for pouch cells [42,43].

In this work we expand upon these previous studies by integrating our unique thermistor array into 4 × 21700 format cylindrical cells, offering temperature measurements with a spatial resolution of 10 mm along the central cavity of the cells. Uniquely we study the cells in a 2S2P arrangement, utilising PLC to communicate sensor data between the cells and a data logging system. Previous reports typically demonstrate instrumentation with single cell cycling (1S) or with bulky data acquisition systems limiting the system scalability [14,39,41,44,45].

Fleming et al. demonstrated instrumenting a cylindrical cell with an optical sensor [41]. This demonstrated the importance of internal cell temperature sensing, but the sensor required bulky logging equipment. In Fleming's study only a single cell was tested, without considering the repeatability of the instrumentation process, nor how the sensors can be used to observe a module of cells. Optical sensors have also been tested by Fortier et al. in this case, with coin cells [45]. Zhu et al. developed a flexible resistive temperature sensor for use with pouch cells. However this again required large apparatus to perform measurements and was not designed to test several cells in a module configuration [44]. New developments, such as wireless transmitters inside li-ion cells, have been investigated, for example Yang et al [39]. These offer promising flexibility to install within a single cell or cells within a module, but in the study published, only 1 cell was tested. Furthermore, there has not been sufficient rigorous testing to demonstrate wireless operation within the environment of a (metallic) battery pack.

Richardson tested a single cell with an impedance analyser during cycling, to show an alternative solution to measuring performance via current and temperature sensing [46]. The relation between cell impedance and parameters such as temperature has been a research topic of great interest in recent years. Electrochemical impedance spectroscopy (EIS) is a proven technique for grading cells based on the response to a range of excitation signals [47]. It is commonplace to analyse the health of individual cells or modules via EIS, which is non-invasive and relatively quick (module grading has been reliably demonstrated within the order of perhaps 3 min or less per device-under-test [47]).

EIS measurements were previously limited to bench-top experiments, where individual cells were tested alone, preventing their use in

real-time nor *in-situ* within a pack. It has been proposed individual cell EIS measurements within a module are possible through integration within an active balancing system [48]. This concept has been further extended, via decoupling ageing and environmental temperature effects from the EIS data, to enable non-invasive estimation of internal cell temperature [49]. EIS is a valuable technique to understanding cell performance, which could be integrated into future smart cell circuitry and included within a collection of on-cell algorithms. Research by Angelis et al. has demonstrated EIS on cells can be performed using similar hardware (i.e. a microcontroller and ADC) already integrated in our circuitry [50]. It is noted extracting parameters such as cell state of health and internal temperature from EIS measurements requires extensive perquisite knowledge, usually obtained from cycling potentially hundreds of identical cells over a period of months [49]; in one case researchers undertook over 20,000 EIS measurements to gather a training dataset for this purpose [51].

In this way, extrapolating temperature estimations would likely require measurements for each type of cell tested. The age and condition of the cell also add variables to the relationship between impedance and cell performance. Our smart cells aim to reduce the processing load on the central BMS, although processing modelling data would be computationally intensive and power consuming for an on-cell processor. Therefore, *in-situ* temperature measurements are required in many scenarios, particularly during the development phase, where the performance of different cells needs to be compared. In industries where device monitoring is critical, such as the aerospace industry for example, cells would likely need to operate over a wide temperature window [52], multiplying the volume of data required to build training datasets. These types of applications would benefit greatly from a complete understanding of cell performance, and proven methods of data collection over a long lifespan.

Optical fibre sensors have been demonstrated to offer high spatial resolution (~2 mm) inside either pouch or cylindrical cells [41,53]. Distributed fibre sensors enable detailed measurements of internal temperature and strain, for example temperature maps can be formed across larger format pouch cells, via weaving the fibre across the front or inside x-y plane of the cell [53,54]. Their thin diameter (<1 mm, including chemically resistive protective sheaf) enables insertion into pouch or cylindrical cells with minimal impact on volume-loss. However, due to their thin construction the fibres are delicate, and currently lack the robustness required for in-operando experimentation outside of a laboratory environment. Long fibres (typically 5 m length) enable multiple cells to be instrumented with one fibre (dividing the high equipment cost), although sacrificing redundancy.

Resistive based sensors (such as thermistors [40][55] and resistive temperature detectors, RTDs [44,56,57], for example the PT100 [43]) have been trialled inside pouch and cylindrical cells. Flexible RTDs have been constructed suitable for internal instrumentation, although the complete system with communication circuitry has not been developed [44]. In this work we measure at 7 points inside a 21700 format cell, compared to previous works monitoring only a single point in a smaller cell [57]. A complete understanding of the temperature gradient within a cell is required to optimise cooling system design.

2.3. PLC network

In this work we use a PLC modem integrated into the electronic readout circuitry to communicate with the data logging system. This network is potentially scalable to cover the hundreds of cells within a pack, without requiring communication wiring. This will enable smart cell integration without increasing weight, volume nor wiring complexity. Our PLC network also allows bi-directional communication, which we plan to exploit further in an upcoming publication. In this case, the master can individually address and control the slave modems, enabling commands to be transmitted to an individual cell. Each cell is given a unique address (contained in a 1-byte variable, thus 255 nodes possible in this configuration), enabling the master to control an individual cell, as well as identifying the data received from each node. Example commands would be to take action (e.g. disconnect from the module) if abnormal behaviour was detected. Wireless solutions, such as capacitive coupling [58], or radio wireless have been suggested as alternative methods of wire-free communication channels [39]. Although wireless channel reception inside the complex metallic structure of a pack cannot be considered reliable without thorough testing in final hardware [59]. Furthermore, wireless technologies are not suitable for real-world systems, due to security concerns (possible intrusive external access [60]) and reliability concerns (external noise factors could degrade signals). These flaws are unacceptable in such a critical system. It has been reported that PLC systems fundamentally can be refined to require lower power consumption compared to a similarly developed wireless system, due to the effectiveness of the transmission over a wired connection [61].

Embedding the sensors, PLC modem and data acquisition/processing circuitry on a cell is a key step towards developing smart cells. As discussed in Section 2.2, the previous works regarding miniatures sensors usually neglect development of a viable data acquisition and communication network, which would help make best use of the instrumented cells for practical development work. Smart cell development in the literature usually focuses on the deployment of a network or link between a cell and a central management system. For example, Lorentz et al. reported on one of the first capacitive coupling system to enable control (active balancing) and sensing (temperature) within a battery module [62]. This system was developed to offer a means of interfacing with a cell without using wires with connectors, which are prone to damage. This was achieved, although there was no comment on the expandability of the system, nor the difficulty of designing a battery pack to contain additional buses to carry the data signals.

The concept of a wireless smart cell has been presented previously in the literature. Initial publications in the area demonstrated, for example, bulky 2.4 GHz radio transmitters, which were difficult to integrate at a single cell level (principally due to the large size of the required antenna) [55,63]. Recently, there has been development of embedded wireless solutions, for example by Yang et al [39]. This included the cycling of a battery cell with an embedded temperature sensor. The proof-of-concept system produced data for the complete test of 100 cycles, although the article did not discuss the possibility to scale-up the concept, nor how to position receivers within a pack or module to ensure robust communications regardless of the cells location within the system. Critically, the ability to be able to send commands to the cell was not discussed. The construction of a bi-directional network is an important step towards developing smart cells. Cells are usually defined as being smart when data can be sent to a master, which can then return a command to actuate a response from the cell (e.g. switching the cell in or out of the circuit for active balancing etc.). Wei et al. summarise the development of smart cell technologies [43]. Embedding sensors inside cells leads towards the development of smart battery packs, although at the expense of additional wiring a complexity regarding BMS development. Smart cells offer a further level of autonomy, where limited actions can be performed without instruction from the master controller. This reduces the load on the BMS, although it requires careful structural design of the battery pack, so the performance of the pack can be maintained, while individual smart cells may be required to limit (or actively balance) their performance.

In the following section we describe our instrumentation process to install a flexible thermistor array, which offers a reliable and repeatable method to instrument cylindrical cells with negligible impact on performance. Our cell cycling experiments verify the performance of the instrumented cells is equal to cells in unmodified condition. We also instrument the cells with a Hall Effect current sensor (located externally) to monitor individual cell currents. This is a further element to aid modelling work and understanding individual cell operation. Quantifying individual cell currents is paramount to understand cell life and

performance. In the literature [64] and our previous work [22], it has been observed currents in parallel cells can converge and diverge during a charge/discharge cycle. To monitor and understand this effect, it is essential to monitor the individual currents through each cell. In this work, individual cell voltage is also recorded. We record data via PLC as well as a dedicated wired USB connection, to demonstrate the reliability of our novel data collection method.

3. Methodology

Our research targets the instrumentation of cells with a variety of sensors (temperature, pressure, gas etc.) with minimal impact on cell performance (capacity, current draw capability, life expectancy). To meet this goal, we have developed a drilling procedure to, in this article, instrument 21700 format cylindrical cells. In many studies instrumenting cells, near complete disassembly of the cell is required to install the sensors [38,41,65], we believe impacting sensor life expectancy and performance, and limiting the scalability of the procedure. We aim to develop our method, so in further work, it could be integrated into a cell assembly procedure, thus enabling sensors to be installed within cells at the point of manufacture. Due to the business confidential nature of our work, we are not able to provide raw data files, and can only present the plots shown in this work.

3.1. Interface circuitry components and sensor selection

Our previous work described the external instrumentation of 8 cells (4S2P arrangement) using two PLC transmitting (slave) modems and one receiver (master) [22]. Here, we provide proof-of concept build and evaluation of smart cells, where each individual cell is able to communicate to the master (i.e., 1 modem per cell). The cells are internally instrumented; the circuitry was miniaturised to a 20 mm diameter PCB, which can fit on top of a 21700 cell can – as shown in Fig. 1, a concept smart cell.

This miniature PCB comprises the following components: a PLC transceiver modem (Texas Instruments, USA, THVD8000DDFR) which costs less than $3 per unit at 1000-unit quantity; a microcontroller (Microchip, USA, ATSAMD21E18A); a dedicated analogue to digital converter (ADC, Texas Instruments, ADS114S08) and a low-dropout (LDO) voltage regulator (Texas Instruments, TPS73133). The ADC provided excellent performance, with a maximum of 12 inputs, all of which are buffered. Furthermore, the ADC enabled high resolution acquisition, up to a maximum of 16-bit, where one bit is used to sign direction. The PLC modem offers communications up to 500 kbps, operating at a central frequency of 5 MHz (which can be adjusted in the range of 1 to 5 MHz). This board was designed to enable PLC at a cell level, however, the board could be customised to facilitate interfacing to several cells, integrating with different sensors (i.e., digital I^2C, SPI devices) or alternatively, a reduced bill-of-materials (BOM) cost version.

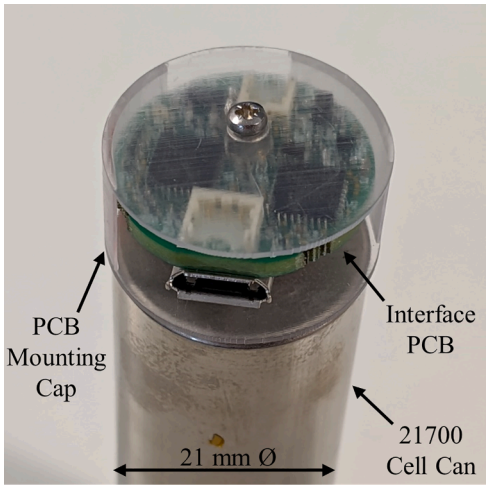

Fig. 1. Concept smart cell - 20 mm diameter PCB installed on-top of 21700 format cell can, with thermistor internal temperature sensor.

In this case, the higher resolution ADC and faster microcontroller were selected to offer detailed sensing, where full ADC resolution was selected, at 10 Hz sampling rate, per each of the 4x cells. A reduced BOM could be devised, for example, using the microcontroller built-in ADC, which would reduce the resolution to 12-bit and would come with the loss of the buffer input measurements, but this could significantly save on BOM cost. The 48 MHz microcontroller, with SPI and multiple UART inputs available, was selected to offer processing capabilities needed for the 10 Hz sampling rate of 9x sensor inputs. A reduced BOM could replace this component with a slower modem, potentially compromising between resolution and quality of data sampling against power consumption and processing speed. The reduced BOM is perhaps suitable for practical applications, where as well as a reduction in cost, the fewer components and lower sampling rates would also reduce power consumption. We propose cell instrumentation will, in the future, be integrated into the cell manufacturing process. The integration of sensors or electronic circuitry will increase the cost of the cells. However their valuable contribution and insights during safety critical applications (e.g. aerospace) or development (low-volume) activities will outweigh these additional initial costs. In this 2S2P configuration (Fig. 2), 1 modem was installed per cell. Of the available 10 ADC channels, 9 were used: 7x thermistor temperature sensors, 1x voltage sensor – measurement directly input from power line, 1x current sensor, per cell. Equally, these channels could be split between several cells – further reducing the BOM per cell, if desired. For example, 3 cells could be sensed via one interface/modem board, if only 1 selected temperature point, 1 Voltage and 1 current measurement were made per cell.

Each cell transmitted data to the external data logger at a 5 Hz sampling rate via PLC as well as dedicated wired USB connection. This USB connection was used only a reference to verify the integrity of identical data transmitted over the PLC network. It is proposed the internal sensors need only PLC to communicate with the BMS. An external thermistor array was installed on the surface of each cell (power and data via USB connection only). This external array was used to demonstrate the usually limited dataset available, when surface sensors are installed on a cell compared to internal core measurements. The 2S2P configuration (each cell 2.5 V to 4.2 V, 5 Ah) provides a maximum voltage output of 8.4 V (10 Ah capacity). In pristine condition, the cell has an impedance of around 24 mΩ (experimentally measured). During normal operation in these experiments, the power consumption of each PCB was measured at 48 mW, reaching a peak of around 150 mW during PLC transmission. This is the worst-case power consumption, where the boards were regularly and repetitively transmitting data, sampling all sensors at full resolution. It is proposed this additional power demand can be reduced by adjusting the sensor sampling rate according to current or temperature events (i.e., low sampling rate when cell is in rest condition). Further power savings could be achieved by optimising component selection for lower power operation, where in this work components were selected favouring high precision data acquisition.

3.2. Sensor design

To avoid increasing the impedance of each cell while monitoring the current throughput a Hall Effect current sensor was selected (ACS37612, Allegro Microsystems, USA). The manufacturer and model of the cell is not disclosed. This Hall Effect sensor was fitted to the bus bar, where a notch was created in the 1 mm thick material. This reduced the width of the bus-bar to around 4 mm minimum diameter at the position underneath the sensor, as shown in Fig. 3. A sensor was installed between each cell and the module. The selected version of the sensor, operating on a 3.3 V supply, has a typical sensitivity of 10 mV/G (Gauss, magnetic flux

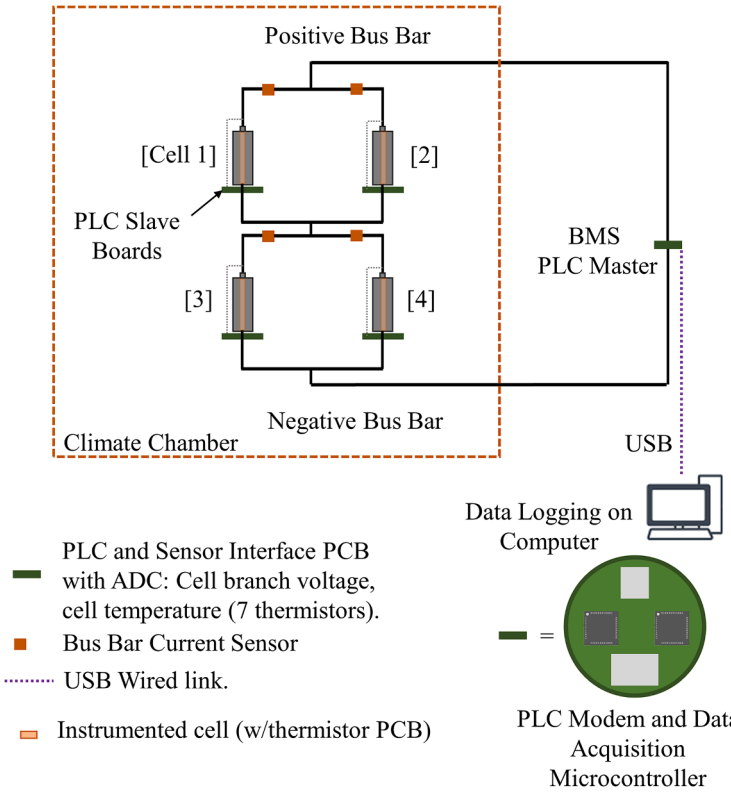

Fig. 2. Schematic of 2S2P instrumented cell setup. 1 PCB (with interface circuitry and PLC modem) and current sensor per cell.

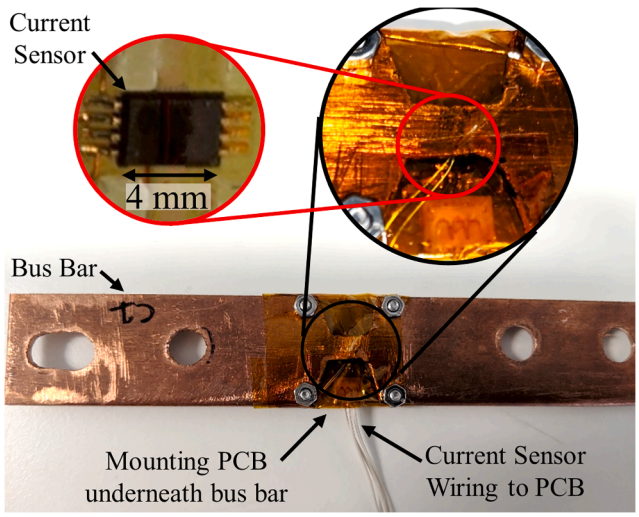

Fig. 3. Photograph of bus-bar mounted current sensor, 1 sensor per cell. Measurement performed via Hall Effect, no added impedance to cell connection.

density) [66]. This unique approach to individual cell current monitoring (without using a sensor in series) merits the use of a high resolution ADC (in this work, currents up to 10 A are expected). Traditionally such Hall Effect sensors are used for applications in-excess of 200 A. The sensor would also be able to measure greater current ranges, if for example, one sensor was used to measure the current through several cells in parallel.

In our study, we demonstrate our custom bus bar design enables accurate measurement of individual cell current (current < 0.5 A, equivalent to C/10). Prior to cell cycling, the sensors were calibrated using a bench-top power supply (HMP4040, Rohde & Schwarz, Germany) and resistive loads (e.g., 1, 2 and 5 Ω); current drawn from supply was instigated via resistance in series. The sensor was reversed to trial current in either direction, as well as line voltage to calibrate voltage sense ADC channel. The calibration procedure is described in full in our previous work [22]. In this previous work, we tested a sensor in series with the cell to measure current flow. However, in this work the measurement system is improved by utilising a sensor which is placed on top of the current-carrying conductor. This avoids adding any additional impedance to the system (i.e. a current sensor in-series may add around 1 mΩ impedance). This reduces sensitivity of the sensor, thus requiring a higher precision ADC to detect small changes in current flow.

The spatial resolution of the internal temperature measurements was defined as 10 mm, along the internal length of the cell. Initial computed tomography (CT) scan images of the 21700 cells demonstrated an empty volume along the centre of the cell (left vacant after removal of the mandrel, during manufacture). This volume stretches the length of the cell, with diameter of ~3 mm. We aim to fit our sensors within this empty volume, avoiding encroaching into the jelly roll or active areas of the cell, to ensure no capacity or capability loss.

To produce a reliable flexible PCB with thermistor sensors, the board must be protected against the corrosive electrolyte inside the cell. Furthermore, the instrument must be inserted through a drilled hole in the aluminium can at the negative end, to allow integration alongside with our cell instrumentation process. Considering these requirements, the maximum PCB width was found to be ~1.4 mm. In this current evolution of the design, a maximum of 7 thermistors could be equally spaced along the length of the cell (centrally positioned in the x plane, Fig. 4(a)), allowing for sufficient track width on a 2-layer PCB. The spatial resolution could be improved via implementing a flexible PCB with internal signal layers, to enable a greater number of devices to be installed within the maximum permitted width of flexible substrate.

Thermistor sensors (100 kΩ nominal, NCP03WF104F05RL, Murata Manufacturing, Japan) were selected, offering miniature size (0201 imperial component size), low cost (cost ~$0.10 per unit, at 1000 unit

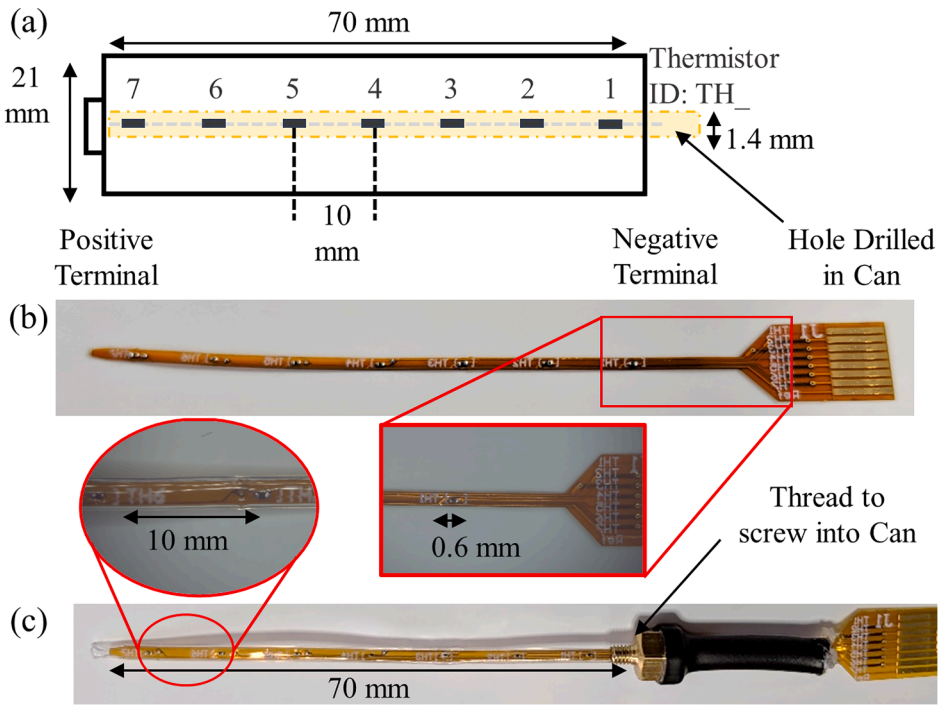

Fig. 4. Development of array of 7x thermistor sensors to insert into cylindrical cell. (a) Schematic of sensor layout, (b) flexible PCB post-sensor soldering, but prior to preparation for instrumentation and (c) final sensor ready for calibration and insertion.

quantity), low current load and suitable sensing range (up to 100 °C). The sensors were attached to the flexible PCBs, Fig. 4(b) via soldering – all components were laid flat to the surface, with a maximum height of around 0.3 mm. The custom flexible PCBs were externally manufactured at a cost of ~$0.70 per board. The dedicated ADC allows every channel to be buffered prior to digitalization, thus the varying resistance of the thermistors during operation did not detriment acquisition performance. The LDO regulator provided the reference voltage for the sensors, where the stable output (low noise) aids precise temperature sensing.

The sensors were protected with a heat shrinkable cover tube, designed to protect against harsh chemicals (electrolyte) and physical damage during instrumentation and cell operation, as shown in Fig. 4 (c). Previous works have protected sensors with conformal coatings [38, 40], such as Parylene. This provides excellent chemical resistance, but the circuitry is still relatively delicate for a manufacturing process, as the coating layer can easily be removed by friction and the thin PCB (<0.2 mm usually, such as our design) is susceptible to tears. In our initial trials, we also found flexible PCBs coated with a conformal coating did not offer precise placement of the sensors inside the cell, i.e., as the flexible circuit 'flexed' and contoured in the cell. Thereby, the sensors were not held in the centre of the jelly roll.

Preliminary experiments were performed to ensure the resilience of the tube coated thermistor arrays against the corrosive electrolyte. Two Parylene coated arrays, two tube covered arrays and two uncoated arrays (bare PCBs, with thermistors attached but no protection) were inserted into vials of electrolyte (one vial per array), with the end two thermistors in each array submerged. The vials were sealed with screw caps; each cap had a hole drilled in the centre to enable the connector of the thermistor array to pass, in a similar way to instrumenting a cylindrical cell. The vials were inserted into a block heater (Techne DB100/2TC) to maintain a constant temperature (25 °C was selected). The arrays were left submerged in the vials for a period of around 5 days, with data logged every 120 s via a bench top data acquisition unit (Keithley DAQ6510). The measured resistances were converted into temperature readings, as shown in Figure 5, where the uncovered sensors are shown in (a), the tube covered sensors in (b) and the reference Parylene sensors in (c). Each subplot contains data from two sensor arrays, where each array is numbered, i.e. [1] or [2] and then each sensor in each array also numbered, i.e. [S1] or [S2].

In these preliminary remeasurements, the thermistors were not calibrated, therefore discrepancy is expected between the block temperature and calculated temperature readings. Importantly, both sets of covered/coated sensors remained stable, following a similar trend throughout. This demonstrates the tube coating was effective during the experiment. The performance of the uncoated sensors quickly deteriorated, with an abnormal drift in temperature observable after a period of only around 100 mins. These experiments will be extended to test the resilience of the coatings over a longer term, as well as across a range of temperatures expected during cell operation (e.g. perhaps up to 45 °C).

In this work we measure the temperature axially along the length of the cell. This avoids major disassembly of the cell, while providing core temperature measurements (thus temperature measurements can be recorded without the delay usually found as the temperature dissipates through the can of the cell). We target axial measurements as indicators for key areas, to help develop effective cooling systems, and also quickly identify hot spots forming in the cell structure.

3.3. Cell instrumentation process

To avoid disassembly of the cell and associated potential performance impact, a unique drilling process was developed for the 21700 format cells. Similar to previous works [67], the negative cap is preferred as the entry point for instrumentation. This avoids disrupting the safety features often included in cylindrical cells (pressure vent) and poses less risk of short circuits (the aluminium can is in effect connected to the negative terminal). In the literature we have not found studies of a repeatable nor automated approach to cell drilling. The drilling of small holes (less than 2 mm) has been reported, but insufficient details are provided regarding precautions against cell damage [46,68].

In this work we create a custom process based around friction drilling. Here, the material is formed and pushed (not cut). Therefore, minimal material loss is achieved (for the construction of the cell and negative current collector). Furthermore, no swarf (dust or waste

material) enters the cell during the process, which reduces the risk of short circuit or contamination within the cell. There is no reliance on magnetism [67], which could drop larger debris into the cell.

Our drilling process uses a mini milling machine (MF70 Proxxon, Germany) selected to offer programmable feed rates and adjustable rotation speeds in a package sufficiently compact for use inside a glove box. This was a sterile argon environment for cell instrumentation, maintained strictly <0.1 ppm moisture and <10 ppm O_2. The friction drilling process, using a 1.6 mm diameter and operated at high drill speed of 9000 rpm and 1 mm/s feed rate, leaves sufficient material to form a thread in the cell end. These drill setup parameters were experimentally determined to offer the optimum hole formation, with minimal damage. A M2.5 thread was selected (created via form tap) to allow sensors up to 1.8 mm diameter to be inserted via custom fittings.

This process avoids the need to permanently affix sensors into the cell (i.e., via gluing, which was found to be unreliable, with potentially substance could leak into the cell). It also enables repeatable instrumentation across different batches of cells. Importantly, sensors can be fully prepared prior to entry into the glove box, allowing precise alignment of sensors, shown in Fig. 4(c). During fabrication the fitting is placed in the desired location i.e., 695 mm from tail of sensor, to position sensors along complete length of cell. The brass fitting is slid over the protective layer and adhesive heat shrink applied above the fitting, to prevent electrolyte leakage during operation. To avoid introducing moisture into the cell, sensors are dried for a minimum of 8 h prior to instrumentation (drying oven, 40 °C under vacuum).

The design of the sensor arrays and complete instrumentation process focused on creating a repeatable method of installing thermistor sensors inside a cell. Importantly the process ensured the sensors were positioned at reproducible locations inside the cell, with minimal impact to the physical cell integrity. In terms of expanding to larger scale production or automation, two key points are noted: (i) no manual placement of glue or sealant is needed during assembly; (ii) sensor components are sourced from off-the-shelf, and flexible PCBs can be fabricated using a standard process. Securing the sensors via a screw fitting enables the sensors to be removed if necessary. This process could be simplified, for example through replacement with a one-time push-fit or rivet interface, which may better suit an automated manufacturing process.

3.4. Instrumented cell formation

The stages from receiving a pristine cell requiring installation of sensors and releasing the complete instrumented cell for experimentation can be summarised as follows. In pristine condition, the cell impedance and voltage are recorded (using a Hioki Bt3564, Hioki E.E. Corporation, Japan). The first reference performance test (RPT) is performed – details of this cycling test are given below. In pristine condition we find most cells from the factory, are received at 30% state of charge (SoC), which equates to around 3.5 V. At the end of the first RPT, the cell is discharged to 10% SoC, around 3.0 V. Inside a glove box the cell is drilled using the forming drill process, and then a thread is formed using the tapping process described above. The hole is then ready to be sealed using a polyamide screw.

At this stage, the instrumented cell can be removed from the glove box (can integrity is preserved, via the sealing screw). The voltage and impedance of the cell is recorded again. The cell is then installed in a test rig, and the RPT is repeated (inside a climatic chamber at 25 °C). The cell is then returned to the glove box, along with the desired sensor. In this case, with a thermistor array, which has been dried in a vacuum oven. The polyamide screw is removed, and the sensor inserted, then screwed into place. A polyamide washer is used to ensure a hermetic seal, as shown in the completed instrumented cell in Fig. 6(a). Side and top views of the cell are shown in Figure 6(b) and (c), respectively.

The instrumented cell is then removed from the glove box, and the voltage/impedance recorded again. The RPT procedure is repeated for the final time, prior to cycling experimentation. Following satisfactory results from the voltage/impedance measurements (meeting the criteria detailed in Table 1) the cell is ready for further experimentation. In this case, developing proof-of-concept cells, to verify the positioning of the sensors, the cells were sent for x-ray computerised tomography (CT) scans (UniTOM XT, Tescan, Czech Republic), performed in-house. The

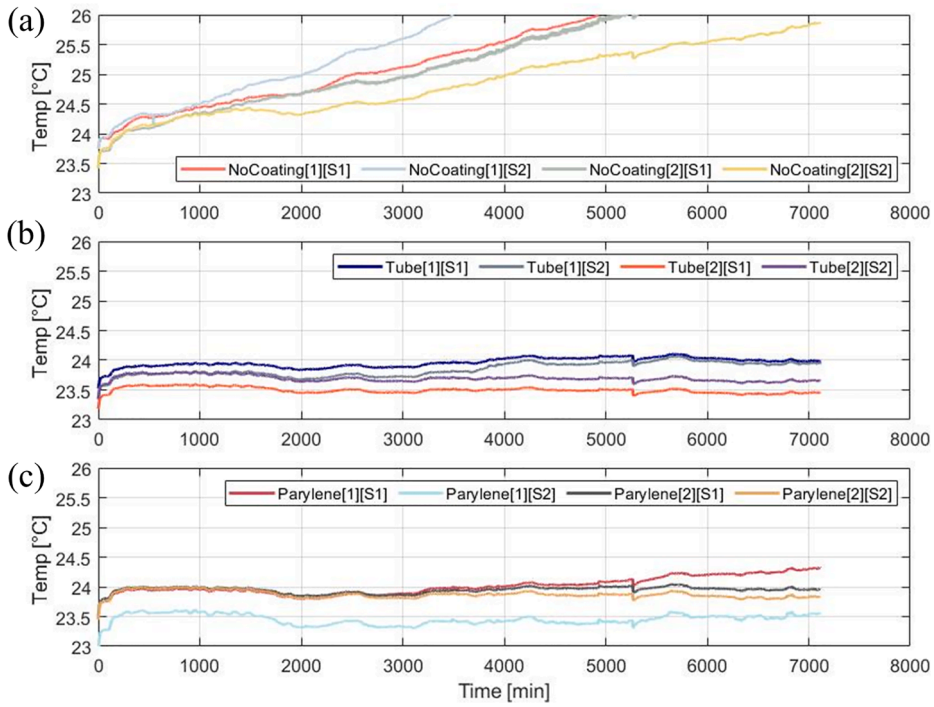

Fig. 5. Preliminary study to verify resilience of thermistor arrays to submersion in electrolyte, (a) unprotected PCB, (b) tube covered PCB (as proposed for cell instrumentation in this work) and (c) Parylene coated PCB (reference).

Table 1
. Success criteria for instrumented cells.

Measurement	Nominal Value	Tolerance	Notes
1 kHz Resistance	24 mΩ	0.5 mΩ	Measured using impedance analyser prior to cell cycling experiments.
Capacity	4.8 Ah	0.05 Ah	Measured during RPT using cell cycler. Capacity measured for each cell when pristine. Manufacturer datasheet notes cells specified as 5 Ah capacity.

sensors are held rigidly in the centre cavity of the cell, Fig. 6(d) and (e), without risk of damage to the jellyroll.

The construction of a thermistor sensor array comprises the following steps (final assembly shown in Fig. 4(c)). The flexible PCBs were designed and fabricated. In this case, 7 thermistors were required per PCB, which were soldered in-house. A basic test, consisting of a simple test of resistance when soldered, and a readout via the miniature PCB is performed prior to further assembly. The PCB is covered with a protective heat shrink tube (a transparent sleeve was chosen, approximately 80 mm length needed to cover the sensors and extend outside of the cell). The tube must under-lap the fitting (with the screw thread) and thus sufficient length is needed so the tube will protrude slightly from the top of the fitting to allow sealing. The tube is then shrunk down with a hot air pencil.

The brass fitting is then passed over the shrunk tubing. The end of the transparent tube is then sealed, via a second heat shrink tube layer (black colour) applied over the end of the fitting and tube. The calibration procedure (detailed below) is performed on each array, with each individual thermistor receiving a calibration output. The calibration procedure involves stepping from 20 to 50 °C (5 °C steps) in a climatic chamber. We accept the sensor as successfully assembled, if temperature aligns with the reference sensors (Type K Thermocouple). The thermistors are expected to be consistently within ± 2 °C minus any offsets etc. Any offsets are removed according to this calibration procedure. The calibration data is stored and recalling during plotting after experimentation. Finally, the sensor is dried in a vacuum oven (40 °C for 8 h), before being ready for instrumentation.

3.5. Thermistor calibration

Manufacture standard calibration, provided with the thermistors, was not sufficient for cell instrumentation (sensors placed on thin flexible PCBs with protective coating could skew the calibration). Each sensor on every completed thermistor array was calibrated against a reference thermocouple (SE027 with TC-08 Picologger, PicoLog, UK). The flexible PCBs were placed in a climatic chamber (MKF56, Binder, Germany) along with associated interface circuitry (USB communication) with individual thermocouple sensors attached within 2 mm. The temperature was incremented in steps from 20 to 50 °C (5 °C intervals, each step maintained for 2 h), to represent the temperature range

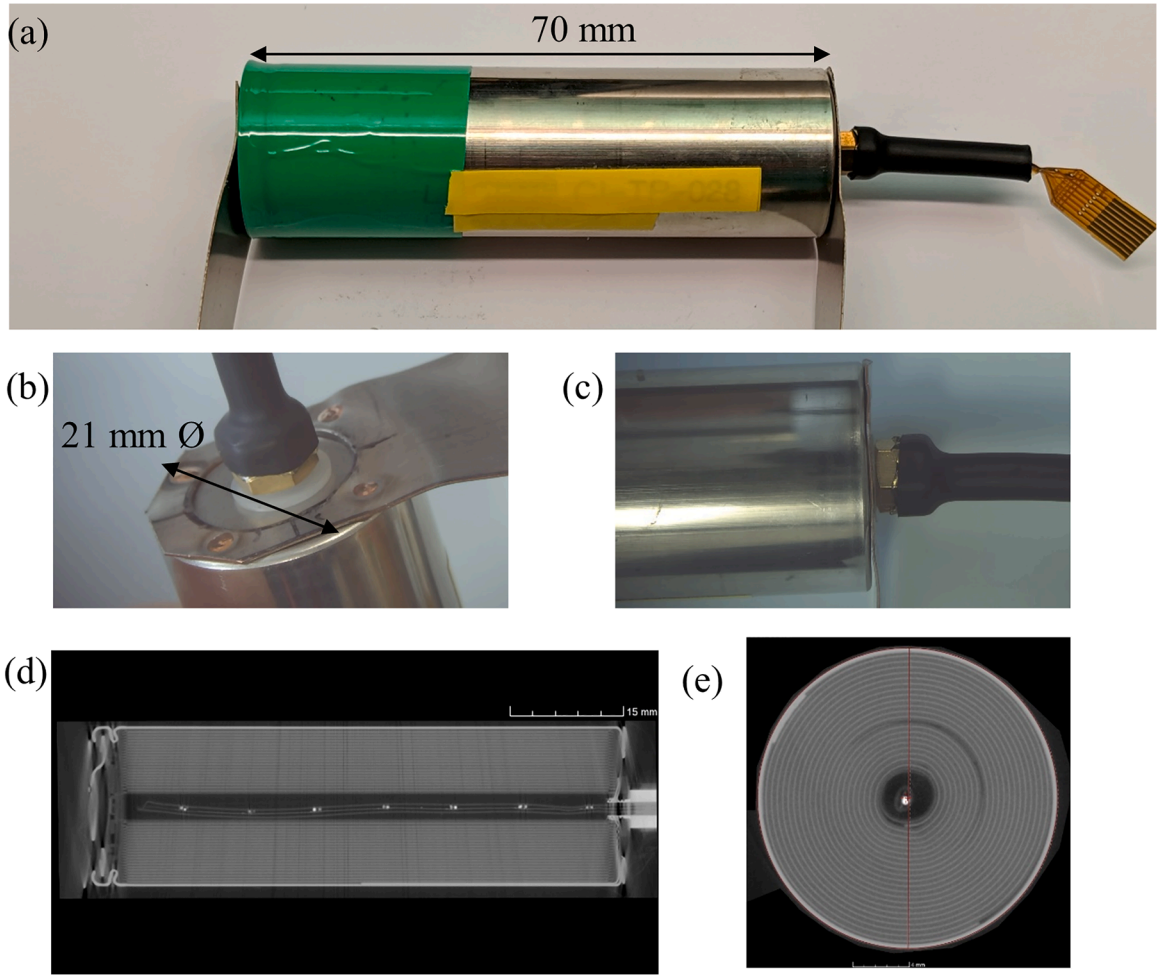

Fig. 6. Photographs of completed instrumented cell (thermistor array). (a) overview of 21700 cell with sensor, (b) top view of sensor showing sensor threaded into cell with sealing washer and (c) side view, fitting flush with can. CT scan images, side view (d) and top-down view on Cell 3 sensor 6 (e) show integrity of cell and jelly roll post-instrumentation.

expected at the core of a cell during cycling. Calibration data (performed in MatLab 2020a, Mathworks, UK via a curve fitting procedure) was calculated for each thermistor. The exponential equation describing the sensor performance was provided on the datasheet, with parameter tolerances set ± 2% and an offset up to 1 °C allowed from factory specifications [69]. Fig. 7. demonstrates the thermistor offset (around 0.5 °C for S1, enlarged view shown inset) is removed through the calibration process (original data using data sheet calibration, data with thermistors calibration procedure applied and reference measurements shown for sensors 1, 3, 5 and 7 in the array).

3.6. RPT

Battery impedance (typically measured with a 1 kHz AC signal) is a typical datasheet metric, and relatively fast (order of a few seconds) measurement (which forms part of our instrumentation process, above). Variation (less than 0.5 mΩ) was permitted to verify cell integrity. It is noted this test alone is not sufficient to comprehensively characterise the performance of a cell [70]. In this work we assess the performance of our cell via RPTs at three stages during the process (cells tested individually): (i) pristine condition (delivered from manufacturer), (ii) Post-drilling (i.e. hole drilled and tapped in can, then sealed) and (iii) post-instrumentation (complete instrumented cell). Here we track the possible degradation of the cell through each step and we verify via our RPTs there is negligible impact on cell capacity (< 0.05 Ah capacity variation) and DC resistance at any stage. Our criteria are summarised in Table 1.

The steps of our RPT will be described in detail in a future dedicated article and will therefore not be repeated here. For completeness a summary of provided for reference. the RPT consists of two static capacity tests (C/1 and C/10) and pulse discharge tests (2C and C/2) at four different SoCs (100%, 80%, 50% and 20%). Each RPT lasts approximately 24 hrs. These RPTs were performed via a cell cycler (VSP-300, Biologic, France), configured with maximum charge/discharge 10 A (2C), compliance voltage 5 V. Here we will focus on the cell energy capacity data to confirm the reliability of the instrumented cells. In a future article we will study the variance and reliability between groups off cells in greater detail. During the RPT (with instrumented cells), internal and surface temperature were monitored, to investigate if any internal fluctuations could be observed (not measurable externally [14]) and to demonstrate the surface temperatures normally monitored are significantly cooler than the core.

3.7. Cell cycling experimentation

To demonstrate the reliability of the sensors and PLC communication setup, a testing procedure was defined as follows, testing the complete instrumented 2S2P arrangement: (i) Pulse discharge stages (similar to RPT, pulses at 100, 80 and 50% SoC, to verify operation with transient pulses of current demand); (ii) 5 cycles of C/2 discharge (cut off at 50% SoC), then C/3 charge cut-off at 4.2 V (to verify PLC operation, and monitor cell core temperature during prolonged discharge), (iii) pulse discharge stage repeated. Experiments were performed using module cycler (FTV 200–60, Bitrode, USA), with the cell SoC not decreasing below 50%. The detailed current profile is shown in the results plots, Fig. 8. shows the instrumentation on each cell, (a) assembled rig with PLC network, (b) enlarged view of single cell, complete instrumentation (internal thermistors PLC, external thermistors USB, single external thermocouple on surface central).

3.8. Drive cycle experimentation

To verify the operation of the current sensor to a transient stimulus, a drive cycle (taken from a real vehicle driving within the urban environment of Coventry city, UK [71]) was scaled (to a maximum discharge 1C). This was then applied to two cells in parallel (VSP-300 cycler). We have presented the scaled current profile in previous work [22]. Compared to the original current values in the drive profile, the module configuration was reduced to 2P in this work, to verify the operation of the sensors and PLC network powered directly from the cell voltage cells with overall voltage varying from 2.5 to 4.2 V. In this case, the LDO regulator was replaced with a buck-boost regulator (MAX20343, Maxim Integrated, USA). The cycle was repeated three times (100%, 80% and 50% SoC across the 2P layout). The list of experiments performed is summarised in Table 2.

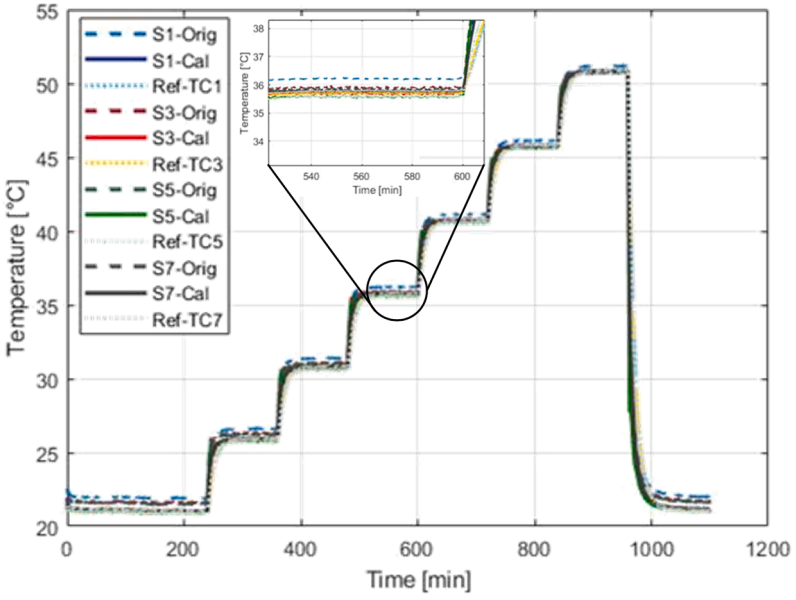

Fig. 7. Thermistor sensors (denoted 'Sx') calibrated with reference thermocouple sensors ('Ref-TCx'), stepped temperature, 20 to 50 °C, via climatic chamber. Each sensor is matched with the corresponding thermocouple (unique calibration generated for each thermistor).

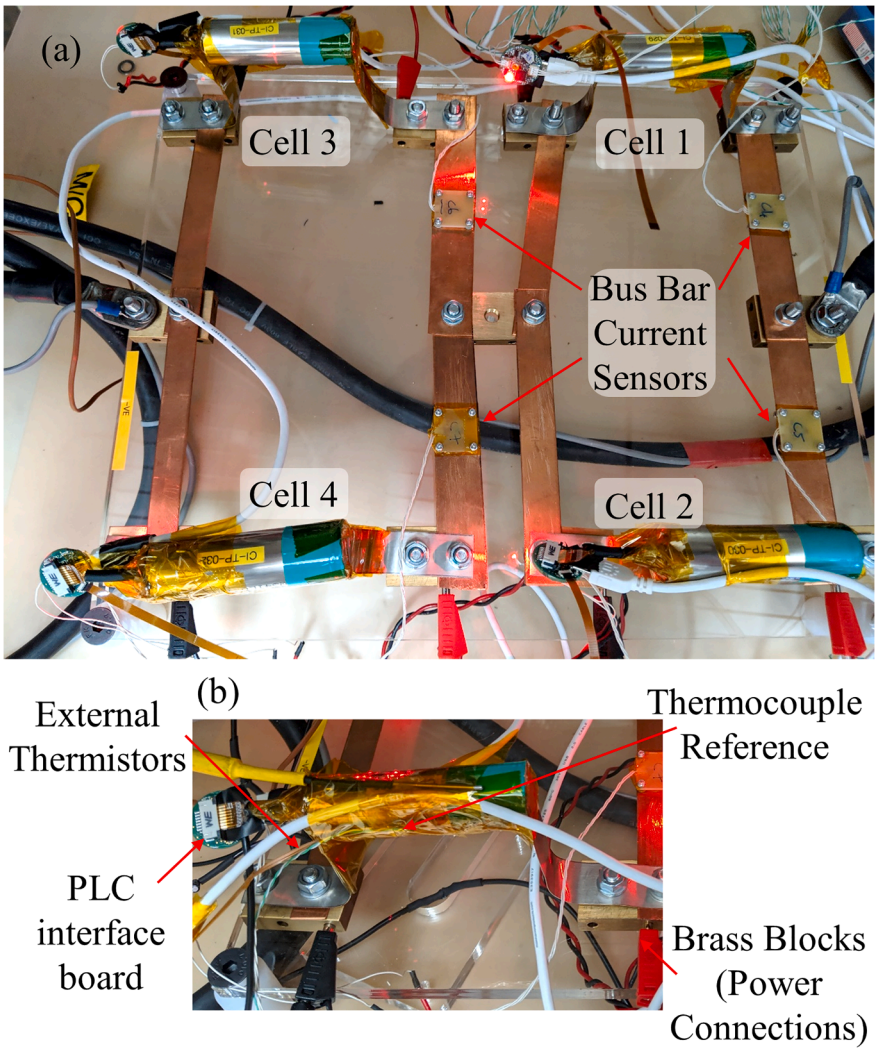

Fig. 8. Photographs of instrumented cell rig, (a) overview of setup with PLC (internal thermistor) instrumentation, (b) enlarged view of fully instrumented cell (internal/external thermistors and reference thermocouple).

Table 2
Summary of experiments and configurations.

Name	Cell Layout	Cycler*	Notes
RPT	Single Cell	VSP	Performed 3x: prior to cell modification, post cell-drilling and post cell-instrumentation. Test serves as benchmark to verify cell capacity and impedance.
Cell Cycling	2S2P	FTV	Repeated 3x. Test used to verify PLC operation during cycling.
Drive Cycle	2P	VSP	Reduced to 2P configuration due to limited cycler compliance voltage. Repeated 3x. Test verified operation of PLC during full state-of-charge range, and with transient current profile.

*Cycler Key: FTV = Bitrode FTV 200–60. VSP = Biologic VSP-300.

4. Results and discussion

4.1. RPT

Prior to cycling experimentation, every cell was reference tested (VSP-300) at pristine condition, post drilling and post instrumentation. The impedance was also measured (BT3564, procedure above), as a precursory check. The results are summarised in Table 3 (capacity) and Table 4 (impedance). Our preliminary measurements noted maximum deviation of circa 2% in cell capacity could be account for by measurement tolerances (for example, quality of connection cell to cycler, apparatus calibration, etc.). Delta capacity listed below refers to capacity lost between pristine condition and post instrumentation measurements. Similarly in Table 4, delta impedance refers to the impedance increase between the two states.

Cells 1, 2 and 4 present similar degradation over the experimental period, with an average 0.2% decrease in capacity. Minor fluctuations in capacity (around 0.05 Ah) are likely due to measurement tolerances. In the future, a revised cell holder for instrumented cells will be developed to ensure a consistent connection to the cycler. Preliminary testing showed minor variation was observed between repeat measurements of the same pristine cell. Slightly higher loss was observed for cell 3, but it was still accounted for by measurement error. The standard deviation for the impedance and capacity measurements shows only a minor

Table 3
Capacity of cells measured via RPT.

Capacity	Cell 1 [Ah]	Cell 2 [Ah]	Cell 3 [Ah]	Cell 4 [Ah]	Standard Deviation [Ah]
RPT 1 (Pristine)	4.828	4.803	4.828	4.792	0.018
RPT 2 (Post Drill)	4.831	4.818	4.764	4.775	0.028
RPT 3 (Post Instr.)	4.823	4.802	4.767	4.769	0.023
Δ Capacity [Ah] (%)	−0.005 (0.10%)	−0.001 (0.02%)	−0.061 (1.26%)	−0.023 (0.48%)	–

Table 4
Impedance of cells, measured via analyser, 1 kHz signal.

Impedance	Cell 1 [mΩ]	Cell 2 [mΩ]	Cell 3 [mΩ]	Cell 4 [mΩ]	Standard Deviation [mΩ]
RPT 1 (Pristine)	23.95	23.17	23.19	23.74	0.34
RPT 2 (Post Drill)	23.89	23.52	23.73	23.57	0.15
RPT 3 (Post Instr.)	23.05	23.65	24.09	23.96	0.40
Δ Impedance [Ah] (%)	0.90 (3.76%)	0.48 (2.07%)	0.96 (4.15%)	0.22 (0.93%)	–

increase in spread is observed throughout the instrumentation process. Considering pristine cells (in ideally identical condition) there is a 0.018 Ah spread and 0.34 mΩ spread in capacity and impedance, respectively. This shows there is a slight variation in cell condition before any testing or instrumentation occurs. Post-instrumentation this deviation has increased slightly to 0.023 Ah and 0.40 mΩ, for the capacity and impedance measurements, respectively. As all four cells remained within our specified tolerances (Table 1), all the cells were considered successfully instrumented. Cell 4 consistently was noted to be lower capacity, from initial tests prior to instrumentation and throughout experimentation.

Minor impedance variation was observed, in the order of less than 0.5 mΩ target, for cells 1, 2 and 4 during the instrumentation process, most notably after the drilling process. In future work we will aim to further refine our drilling process, to ensure minimal damage or reduction in available material on the internal current collector and welds. Cell 3 was noted to increase by just under 1 mΩ. As this is a manual process, where probes are needed to connect the cell to the measurement equipment, variation in contact point, and force applied potentially influenced measurements.

During each RPT sensor data were logged, an example subset of data from cell 2 is shown in Fig. 9, showing (a) voltage, (b) current, (c) external and (d) internal temperature measurements (data acquired at 5 Hz sampling rate). Here, these measurements are relative to ambient/baseline temperature readings of approximately 25 °C, inside climatic chamber. In this experiment, voltage and current data were recorded via the cycler only, due to the lack of connection to the power line, and all temperature data were logged via USB. This enabled the interface boards to be powered from the data logging computer, which prevented variation in power demand from influencing the capacity measurements.

A large variation between internal and external temperature data is observed throughout, notably peak variation of ~2.8 °C. The 1C discharge causes a peak increase in core temperature, where the hottest temperature was observed by sensor S7 located close to the positive terminal. A maximum peak of around 14.7 °C increase above ambient was observed, with similar temperature also observed for cell 1. In the surface temperature measurements shown Fig. 9(c), peaks due to higher current charge/discharge can be observed, although at lower magnitude. The internal sensor data contains a greater detail of information regarding cell performance. For example, different temperature increments are observed at the individual SoCs (when subjected to the 2C discharge during the period of 800–1300 min). The internal sensors detect a peak 1.5 °C rise at 100% SoC, compared to a greater peak of 2.1 °C above ambient, at 20% SoC. The surface sensor data demonstrates only a minor variance, of 1.3 and 1.4 °C peak increases, during the 2C pulse at 100% and 20%, respectively. To verify the internal sensors did not effect the operation of the cell, nor temperature distribution, an unmodified (pristine) cell was fitted with only external sensors. The RPT was performed on the cell, as shown in Fig. 10.

The gradients observed during the RPT are within expected

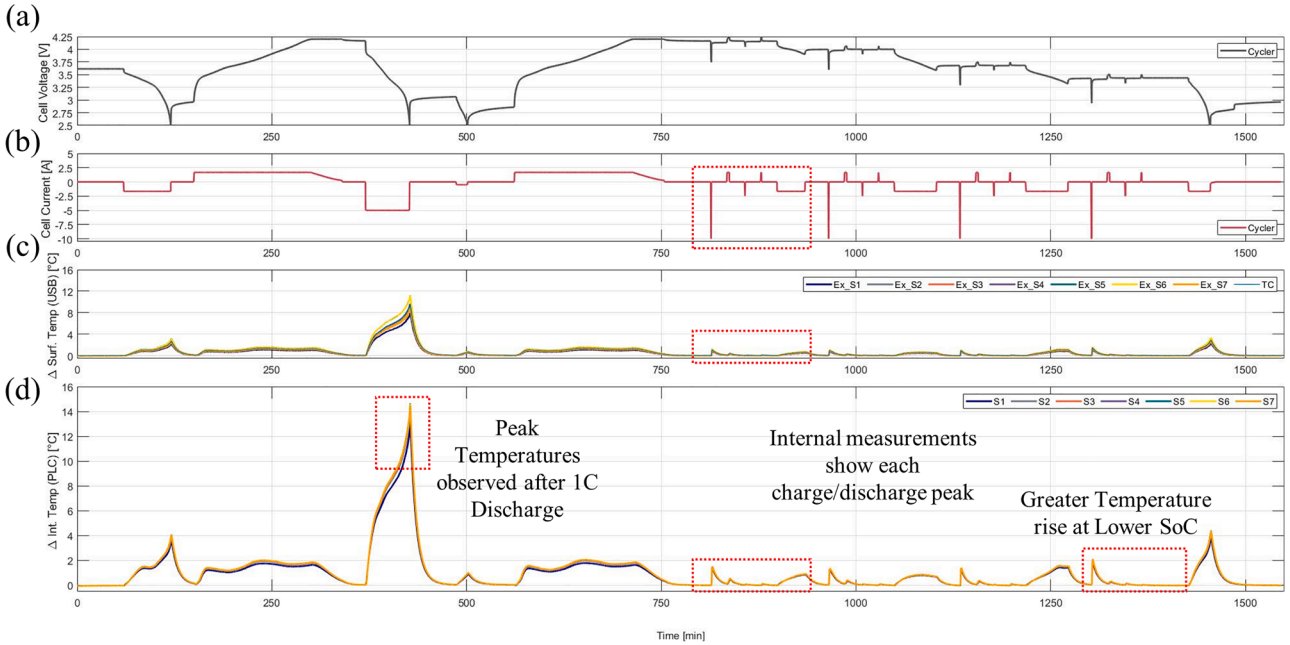

Fig. 9. Typical sensor data monitored during RPT for a typical instrumented cell, (a) voltage, (b) current, (c) external temperature and (d) internal temperature. Wired USB connection used for communication.

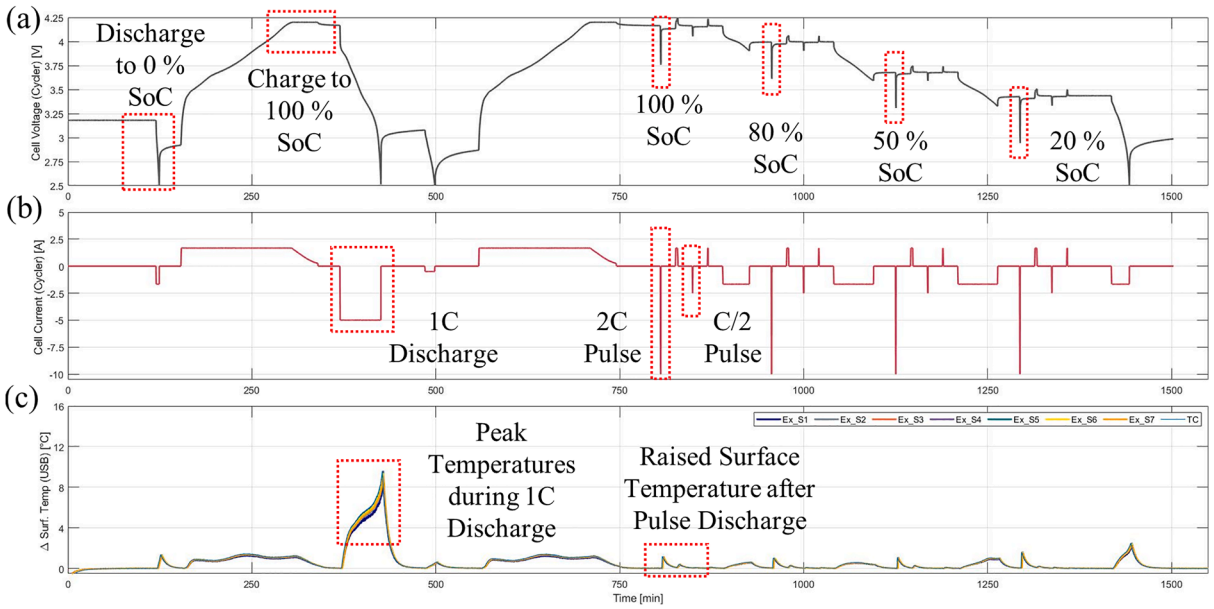

Fig. 10. Typical sensor data monitored during RPT for an unmodified cell, (a) voltage, (b) current and (c) external temperature (thermistor array attached to surface of can, no other instrumentation fitted). Wired USB connection used for communication.

tolerances to those observed with the instrumented cells. The variance in temperature for both the instrumented (Fig. 9) and unmodified cell (Fig. 10) generally follow a pattern where coolest temperatures are observed near the negative terminal, with hotter areas recorded closer to the core and positive terminal of the cell. This demonstrates the temperature profiles in the cell are not greatly influenced by the sensors placement in the cells. In both the instrumented and unmodified cells, a peak temperature of around 10 °C is observed, demonstrating the thermal performance of the cell is not noticeably affected.

It is noted in some cases during preliminary testing, minimal features were visible on external sensor data, and greater delta internal vs external data. This demonstrates the poor reliability of attaching an external sensor, and the uncertainty introduced by measuring effectively the external surface between the usually hotter cell core, and surrounding environment. External sensors are also prone to damage during cell transportation. When installed correctly, internal sensors offer reliable data, without requiring bulky sensors located around the radial outside of the cell housing. The variation between internal core and surface temperature measurements aligns with data in the literature; larger variations (5 or 10 °C) have been reported [14,46], dependant on SOC, current profile and magnitude.

4.2. Cell cycling

The 2S2P module was cycled with our test procedure for three repetitions – representative data from one repetition is presented here. During these measurements data were logged via PLC (internal temperature, voltage and current) with the circuitry powered from each

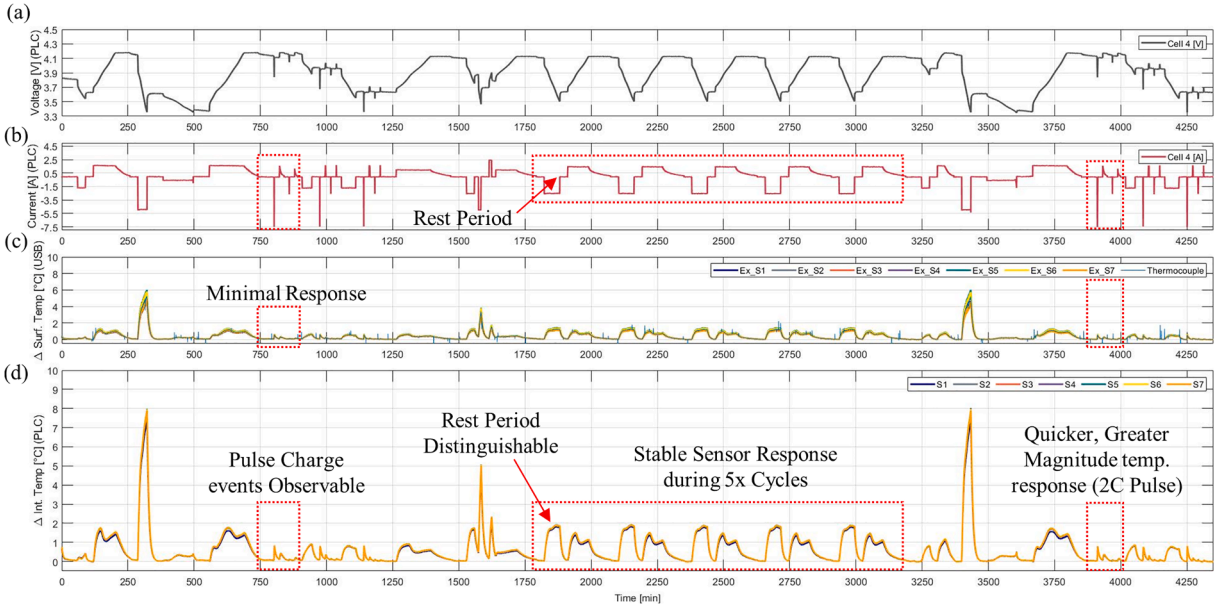

Fig. 11. Instrumented Cell 4 data, showing PLC logged data (a) voltage, (b) current and (d) internal core temperature, with (c) external can temperature (temperatures relative to baseline value ~25 °C).

individual cell; an external thermistor array was installed on each cell, radially aligned, and logged via USB. To align the sensors, the internal and external sensors were positioned to face inwards and outwards, respectively. The orientation of the sensors was observed via CT scan data, and visually during operation, via the orientation of the flexible PCB (the connector of this board is directional and only present on one side of the board). Temperature data is reported in degrees Celsius above ambient climatic chamber set-point (25 °C – baseline temperature taken for each sensor prior to experiment).

Typical data from a single cell (designated cell 4) is shown in Fig. 11. In these plots, data were logged at 5 Hz continuously from each cell. Reference external temperature data, measured via a thermocouple and Picolog equipment, were logged. The point measurement probe was located closest to S4 on the external array. Fluctuations in temperature can provide early warnings to cell failure. The internal measurements shown, Fig. 11(d) compared to external (c), demonstrate small changes in temperature (<0.5 °C internal) are not observable externally; consistent with previous findings [14].

The internal core temperature data for cells 1,2 and 3 (Fig. 12, a–c, respectively) follows similar trends, where the sensors towards the positive cell terminals (S7) exhibit hottest temperatures. This highlights the importance of temperature measurements in addition to current and voltage readings, where peak temperatures are observed following a 1C discharge. For example, at points circa 250 and 3430 min experiment time, the peak current demand (1.5 C for 1 min) causes a minor temperature rise (< 1 °C).

The peak temperature observed during cycling alone is not representative to the cell capacity degradation, nor performance of the cell. The temperature gradient along the length of the cell can influence cell ageing and degradation [12,34,38]. An enlarged view of the peak observed temperature during this cycle (around 3400 min experiment time), Fig. 13, (a)–(d) for cells 1 to 4, respectively, demonstrates minimal gradients. These gradients were measured as <1.2 °C at a peak temperature increase of almost 8 °C above ambient. It is concluded insignificant gradients are present in this early stage of cell lifetime; here lifetime to this point consists of 3 RPT studies, 3x experimentation cycles and 3x drive cycles. These results are summarised in Table 5. In general, the consistent cell performance is further evidence of a robust and repeatable instrumentation process.

Cell 3 has been observed to decrease to the lowest capacity post instrumentation (4.767 Ah) and does not exhibit the greatest magnitude of temperature increase. However, cell 3 does show the maximum temperature gradient (S7 hottest to S1 coolest, 1.2 °C temperature delta, relative to maximum 7.9 °C increase), demonstrating a larger gradient is forming. In future work, these instrumented cells will be aged. It is proposed the cells will be fully charged and discharged across around 100 cycles or when the state of health has reduced by approximately 20%, to observe if these trends magnify.

To verify the performance of our bus bar current sensors and voltage readout, these data were compared to the reference values recorded by the cycling equipment. Individual values for each cell were logged, example shown Fig. 11(a) and (b) for voltage and current, respectively; for comparison with the overall module (2S2P) readings logged, the values have been summed in series and parallel for voltage and current, accordingly. For example, module voltage is calculated by summing the series chains of cells 1 & 3 and 2 & 4; module current via summing cells 1 & 2 and 3 & 4. The data shows excellent response compared to the cycler (FTV 200–60); Fig. 14 shows (a) current data and (b) voltage data.

The bus bar current sensor is capable of measuring minor current fluctuations (< 1 A), demonstrating with our bus bar notch design, the sensor has successfully been calibrated to an appropriate range for 5 Ah cylindrical cell testing. The small sensor (package 3 × 4 mm) is suitable for installing on smaller bus (notch 4 mm width or lower) bars, enabling contact free measurements in compact module designs. The 16-bit resolution ADC is appropriate for laboratory measurements; a lower cost, smaller PCB would be possible if lower accuracy and precision could be accepted via the inbuilt microcontroller ADC (relying therefore on unbuffered, 12-bit inputs). Excellent voltage resolution and sensor readout precision has been achieved, demonstrated via the inset voltage plot, Fig. 14(b). This shows stepped bit levels in cycler data records at

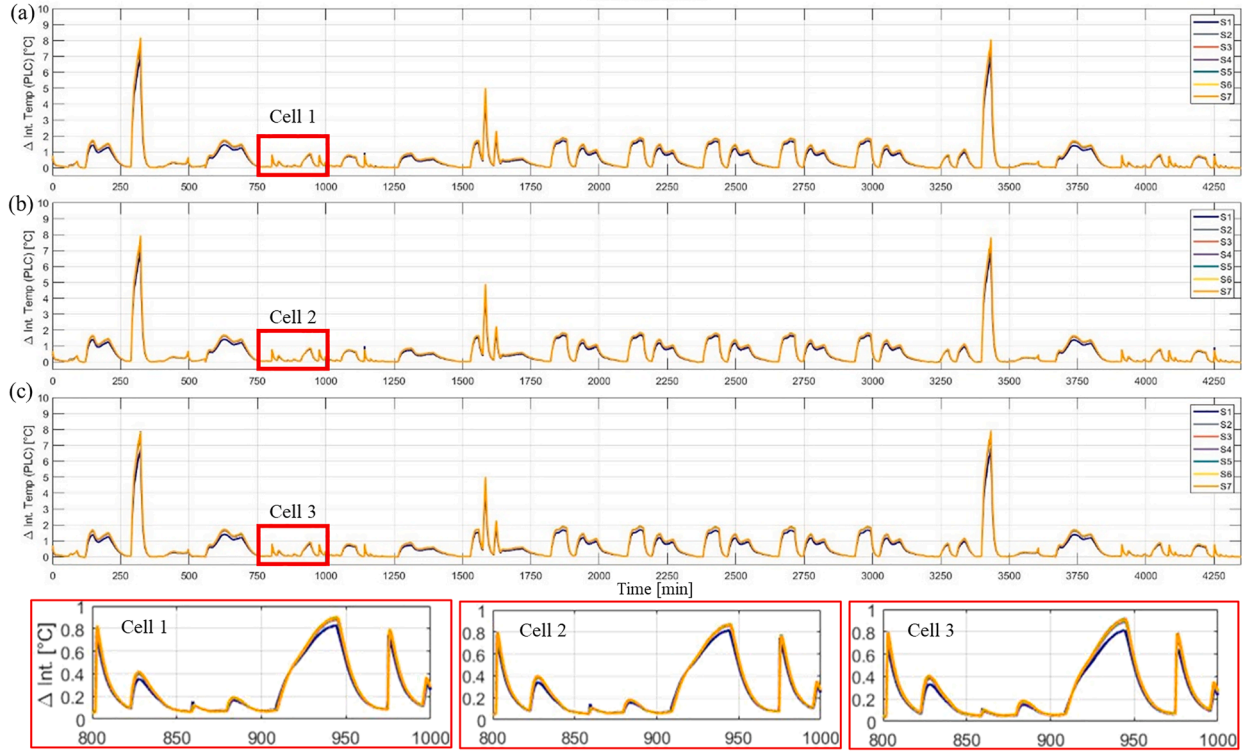

Fig. 12. Internal temperature data (via PLC) logged for cells 1 (a), 2 (b) and 3 (c). Inset plots show temperature rise C/3 (30 min duration, ~940 min experiment time) compared to 1.5C discharge (1 min duration, ~970 min experiment time).

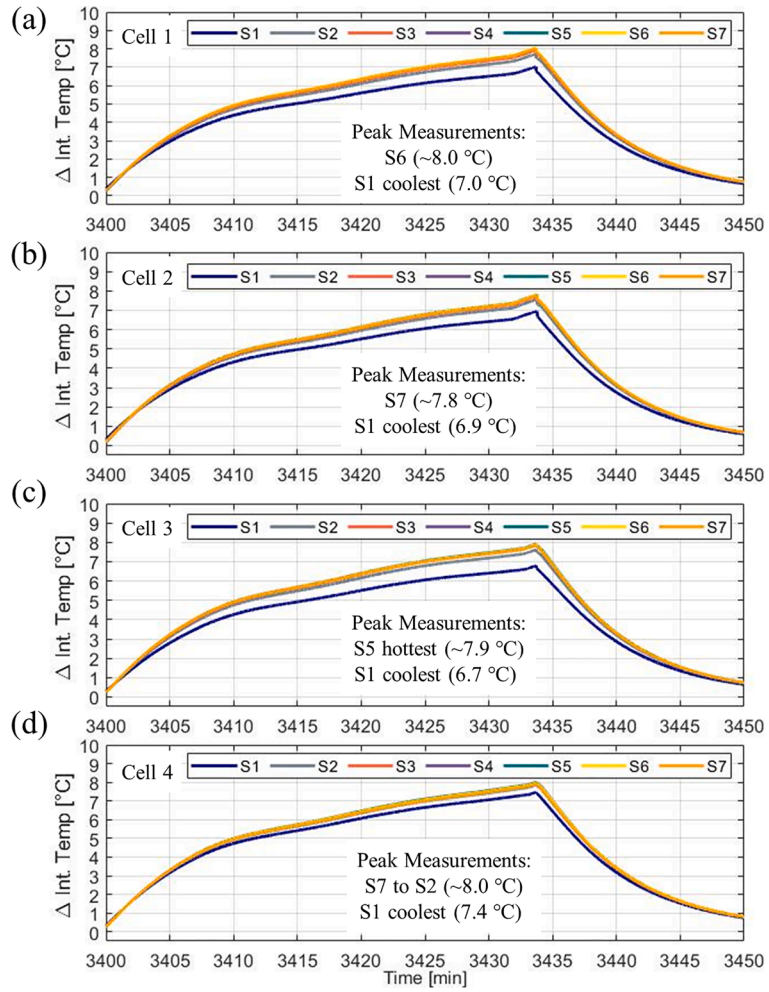

Fig. 13. Enlarged view of 50 min period of experiment, peak temperature observed for cells 1 (a), 2 (b), 3 (c) and 4 (d). Minimal temperature gradients observed for cells.

Table 5
Summary of peak temperature and gradients measured during cycle.

Measurements at peak temperature after 1C discharge (end of cycle, 3430 min interval)	Temperature [°C above ambient] (Hottest Sensor)	Temperature [°C above ambient] (Second Coolest Sensor)	Temperature [°C above ambient] (Coolest Sensor)
Cell 1	8.0 (S6)	7.6 (S2)	7.0 (S1)
Cell 2	7.8 (S7)	7.5 (S2)	6.9 (S1)
Cell 3	7.9 (S5)	7.6 (S2)	6.7 (S1)
Cell 4	8.0 (S7 > S2 within 0.1 °C)	NA	7.4 (S1)

the 890 min location, where voltage is exponentially decreasing, verified by miniature sensor output. Inset current plot, Fig. 14(a), demonstrates fast sensor response, where the sensor response is time aligned with step changes in current application. To further analyse sensor performance, drive cycle data is presented below, to verify transient response.

Data were logged via USB, with a dedicated wired connection (1 cable required per cell) for all sensors (internal temperature, current, voltage) for comparison against the PLC network Fig. 15. demonstrates identical data received for voltage (a), current (b) and temperature (c). Zero errors were found, as shown in plot (d). Minimal time difference was noted when comparing the time data was received via the reference wired USB connection and the PLC link. It is noted in this experiment, a computer was used to record the message time received. This introduced an undeterminable offset into the timestamps, as the system was not optimised for real-time data logging. In preliminary experiments we note a time delay of < 30 ms is expected.

Data were logged for a period of nearly 4300 min (5 Hz sampling rate per cell, 4x cells) successfully, with identical data logged via dedicated connection. During this experiment, the complete 16-bit ADC resolution data set was maintained. In this period, around 12.5 m messages were received in total, requiring storage in a file consuming over 1 GB in size. These experiments expanded our initial proof-of-concept study [22], and vastly expand upon the limited data transfer capability previously reported in the literature [72,73]. Further experiments reported separately in a later article focused on the PLC element, will demonstrate comparable performance to a CAN bus, in terms of baud rate and reliability. Advantages of PLC compared to a CAN, include reduced complexity (no ground isolation required), lower power consumption, less wiring (PLC uses bus bars) and reduced weight. The miniature low power consumption, low voltage components selected, demonstrate the technology is available for PLC modem and acquisition hardware to be appropriate size for smart cells.

4.3. *Drive cycle (operation over full SoC)*

To verify operation of the PLC system over the full cell SoC (2.5 to 4.2 V) and to validate the current sensor with a transient profile, a vehicle drive cycle, described above from [71], was repeated for four

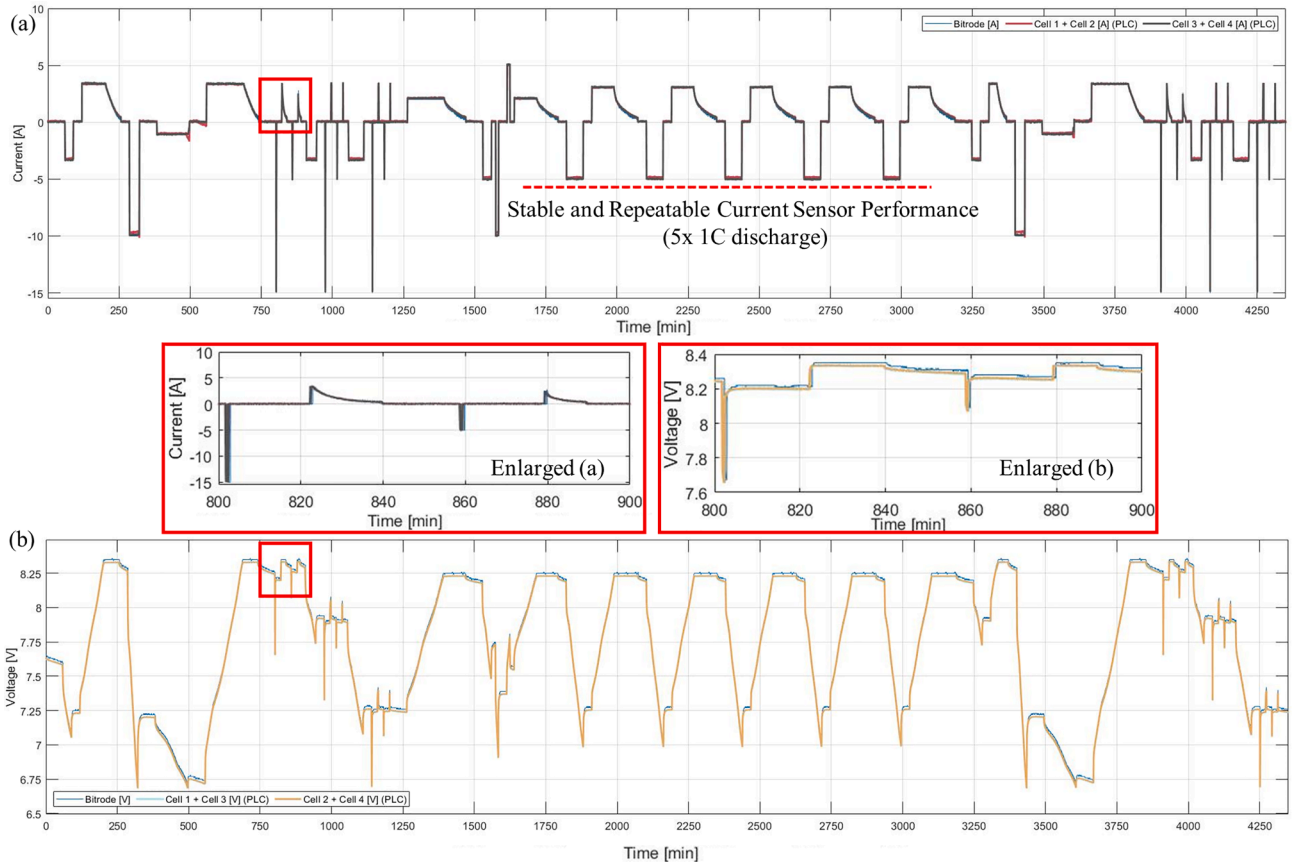

Fig. 14. Data recorded overall from 2S2P module, (a) current and (b) voltage data. Summed individual cell data (logged via PLC) with bus bar Hall Effect current sensor and 16-bit ADC compared to cycler reference measurements.

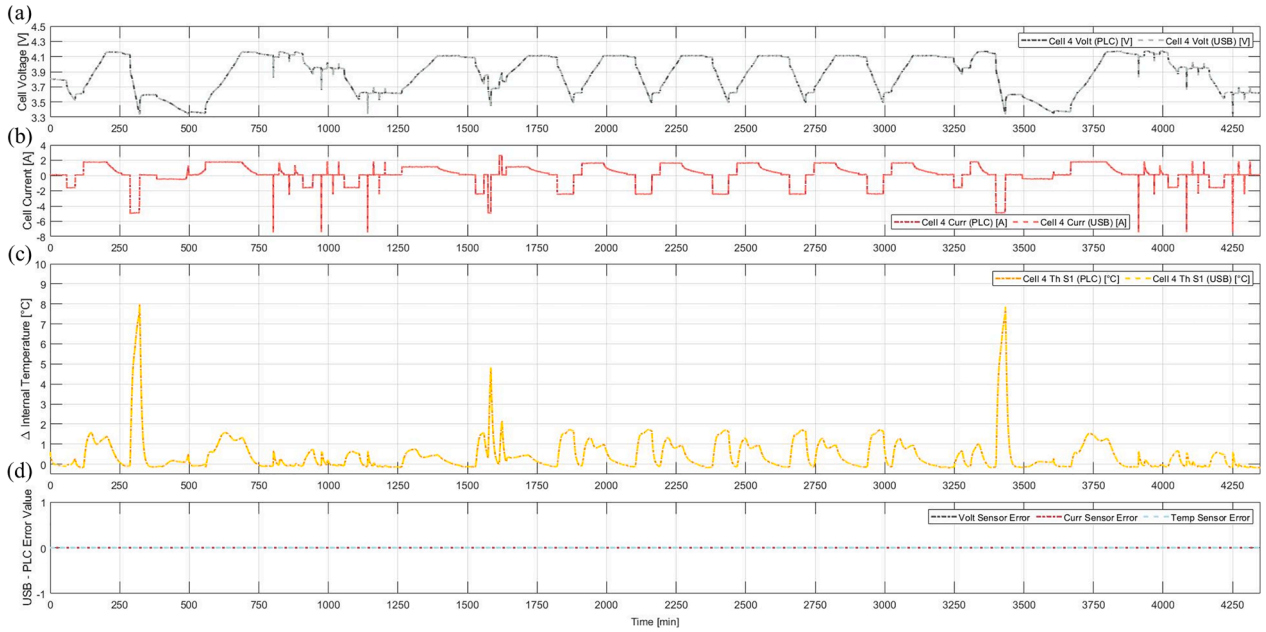

Fig. 15. Reliability and capability of PLC network verified against reference dedicated wire connection (USB), comparison of (a) voltage, (b) current and (c) internal temperature data from cell 4. Zero errors demonstrated in this period (5 Hz sampling rate), (d).

SoCs (100%, 80%, 50% and 30%). Here the SoC level was set via charging or discharging to a voltage after the previous cycle. The SoC voltage was determined for this cell type via the initial RPT studies. Here, cells 1 and 2 were taken from the experimental setup shown in Section 3 (remaining in parallel thus, 1S2P). The cycling equipment selected for the RPTs was primarily targeting single cells to be tested individually, so did not permit the higher compliance voltage needed to maintain the 2S2P layout. The PLC network was powered entirely from

the cells, via buck boost regulators (logging rate set to 10 Hz). Data were logged via PLC for cells 1 and 2, as shown in Fig. 16(a) and (b), voltage and current, respectively. Data for cell 1 external (USB thermistor array) is shown in Fig. 16(c) with corresponding internal temperature data (PLC) shown in (d).

Hotter temperatures were observed at the lower SoC cycling, with a peak nearly 4 °C rise for S7 at 30% SoC cycle, compared to 0.8 °C S7 at 100 and 80% SoC. Note, in the current sensor plots, the cell current is half the current value recorded by the cycler; this is due to the cells parallel configuration, meaning the current path is split between the two cells (therefore the sum of both current sensors will equal the cycler recorded current). The current sensors demonstrated excellent performance the transient (and less than 1 A) current variation; inset plot, Fig. 16(b), demonstrates fast data logging during initial 5 min of drive cycle. The enlarged plots demonstrate the current sensor (b) responds rapidly to a transient drive profile, while there is no crosstalk or degradation in the thermistor measurement system, shown in enlarged plot (d). The PLC network maintained reliable communication with the master node throughout the experiment, where zero errors were detected. The experiment was halted by the cycler when the cell reached minimum SoC (2.5 V).

5. Conclusions

Our unique instrumentation process, via friction drilling and thread forming, has been proven to provide a secure, reliable and repeatable method to internally instrument cylindrical 21700 format cells (5 Ah cells tested). Our RPTs and thorough investigation, sample of CT scan images Fig. 6(d) and (e), demonstrate the minimal impact on cell performance (capacity and resistance measurements taken). On average, cell capacity decreased by only 0.47% during the entire instrumentation process, which was verified pristine, post-drilling and post-instrumentation RPTs.

The fabrication of thermistor arrays (7 sensors, fitted 10 mm apart on flexible PCBs) outside of the restrictive environment of a glove box, enabled precision and reproducible arrays to be developed. The development of custom brass fittings with screw thread provided a means to securely install the sensors within the modified cells. The standard M2.5 thread avoids use of glue during instrumentation and provides a platform to expand the range of sensors internally installed within the cylindrical cells. A chemically resistant heat shrinkable tube was preferred to offer protection (physical against friction damage during insertion) and chemical (electrolyte during operation), compared to a conformal coating. Internal CT scan images showed the tubing also maintained the physical structure of the flexible PCBs; thus sensors were placed precisely in the centre of the cell mandrel, without the risk of introducing twists or crushing.

The RPT test included a peak discharge of 2C, demonstrating the greatest rise in internal temperature (cell 2, hottest S7 14.7 °C above 25 °C ambient, thermistor nearest positive terminal) and cementing the need for internal measurements (corresponding external sensor reading ~2.8 °C lower). This shows internal sensing provides vital cell performance information, such as core temperature and location of hotspots. Previous internal sensing was not suitable for deployment in modules, i.e., not usable for development and testing work, as cabling required (affecting physical volume of the module) to interface with sensors.

Our novel PLC network avoids the need for cabling within the module, although in this work, for data integrity checks, reference wired measurements were also taken. Without bulky cabling, realist module structures can be formed. The PLC network demonstrated excellent performance, with zero errors detected compared to dedicated wired USB reference.

The PLC system was further tested over the full SoC of the cell (2.5 to 4.2 V), where the LDO (operating above 3.3 V) was replaced with a buck-boost regulator. A drive cycle was used to test the transient response of the sensors; excellent performance was observed, with no

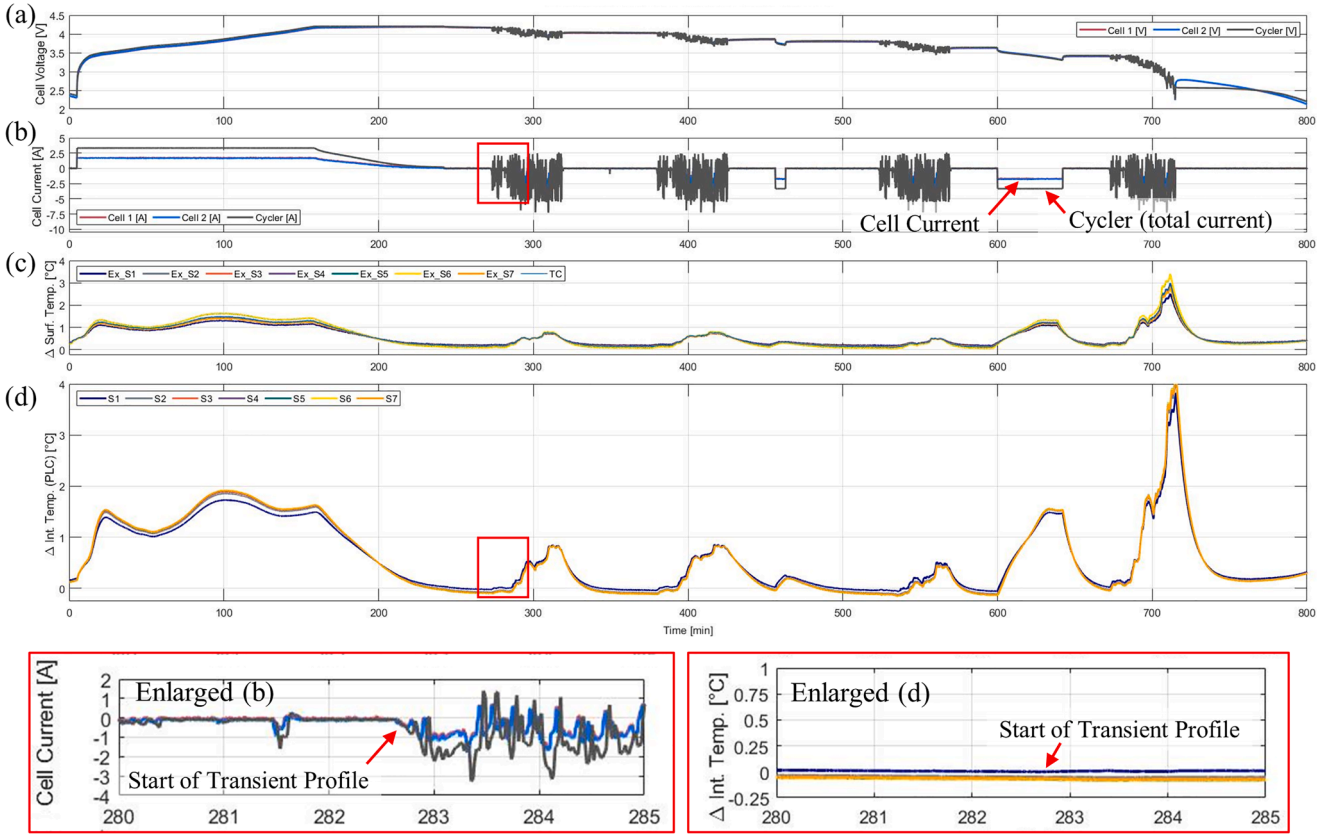

Fig. 16. Drive cycle profile tested with cells 1 and 2, (a) voltage, (b) current, (c) external and (d) internal temperature measurements.

erroneous spikes or data points found during the 800 min experiment. This consisted of a drive cycle repeated four repetitions, at 100%, 80%, 50% and 30% SoC. A peak temperature increase (positive terminal thermistor S7) of 4 °C was found, during the lowest SoC cycle.

The reliability of the PLC system has been proven, however the system would need scaling up to suit battery packs of modules containing tens or hundreds of cells. There is no strict limit to the number of cells in the PLC network, but it is acknowledged additional sources of noise and interference will be present in a real-world application. The miniaturisation of the traditionally complex circuitry and wiring, offers improved deployment in developing and testing environments, easing the placement of cells within prototype module layouts. The circuit could be simplified further, with a reduced BOM, although at the expense of ADC resolution and precision. In this way, the PCB in this work was designed to capture data from a thoroughly instrumented cell, at 16-bit resolution. Trading off the sampling capabilities would reduce the BOM cost, and likely reduce the power consumption (~48 mW in standby).

This work has demonstrated our smart cells, instrumented with thermistor, current and voltage sensors, and incorporating a novel low-bandwidth PLC system are ready for further experimentation and verification, leading to data aiding cell modelling and pack development.

Further work

The creation of a secure fitting (via M2.5 thread) presents opportunities to reliability install other sensors (e.g., pressure, reference electrode) into the cylindrical cells. The flexible PCBs can be protected against corrosion; it is proposed additional sensors (e.g., miniature digital sensors) can be integrated within a cell. This will enable redundancy or perhaps precise sensing at a desired temperature range, or operation at an extended range, beyond 150 °C, which is the current limit of these thermistors. It is noted, the methodology behind protecting the thermistor arrays, via protective coating or covering, will be directly transferable to other cell formats, such as pouch or prismatic. With different cell constructions, the drilling/forming process will need adaptation to suit the format. The sensors, interface circuitry, PLC network and flexible PCBs will need only minor modifications.

The integrated circuity and communication systems on the cells are key to our goal of developing smart cells. This future work goes beyond integrating the sensors into the cells, and also includes developing the processing algorithms needed to interpret data without overloading the BMS with raw signals. Given this processing capability with precise sensor data available on a smart cell, this presents opportunities to integrate features such as EIS into the cell. Further understanding of cell performance or control systems (such as active balancing) are more readily available through smart cells.

We aim to investigate further the impact of our drilling process on the internal current collector, to minimise damage or material loss; in this work, approximately 0.5 mΩ increase in cell impedance was observed after the drilling procedure. We believe it will be possible to integrate our method into the cell construction process, thus enabling sensors to be installed at the point of cell manufacture.

In this work the process of cell instrumentation has been verified and the sensors demonstrated to provide insightful data. These instrumentation procedures and sensor construction is ready to support modelling work and pack development work. In future work, the data collected from surface and internal sensors can be compared with cell models for validation of the theoretical data.

It is acknowledged the developed cells in their current state are at the proof-of-concept stage, where further development work would be required to prepare the technology for volume production. A key point during the conceptualisation of the instrumentation process was to avoid the use of glue or the application of any material that would be challenging to scale-up or that would impair the operation of the cell. In this way, the developed instrumentation procedure would require refinement for production readiness, but fundamentally demonstrates a robust/reproducible method to instrument cells. Similarly, the internal measurements were only performed axially, to avoid substantial disruption to the construction of the jelly roll. If radial measurements were desired, the sensors would likely need integration into the jelly roll build-up (and could not be integrated into a cell post-production).

The PLC system has been proven reliable (zero errors versus reference USB connection) but could be optimised further to improve ease of scalability. Only one transmission frequency is tested here, where it is proposed one frequency is used for general data transmission (normal operation) and a separate channel (frequency divided) is used for priority messages that may be sent when sensors detect the cell is operating outside pre-defined parameters. Our next steps will include testing the PLC network and data collection methodology with a larger module. We also propose logging the data via a dedicated real-time system, to avoid the errors noted when using a standard computer to record the time-stamp data was received. This will allow a reliable indication of any delays introduced when sending data via PLC compared to a reference dedicated wired interface.

The RPT measurements demonstrate minimal impact during instrumentation on cell characteristics, although this progress must be tracked over the cells lifetime. Our next experiments will include ageing data, for example 100 cycles over a 1-month period or when the State of Health has reduced to circa 20% with intermediate RPT studies. This will allow comparison to published ageing data, and thus verification instrumented cells offer equal performance to pristine counterparts. Longer term studies will also be performed on the flexible sensor array, to verify resilience to electrolytic environments over a period representative of a cell lifetime.

The cell rig design shown in Fig. 8, limits the benefits of smart PLC instrumented cells, where inter-cell interactions are not observable (i.e., cells in a module are located physically close). It is proposed a new rig and tab designs would enable a compact system, to house cells in close proximity to enable investigation of realistic module designs.

CRediT authorship contribution statement

Timothy A. Vincent: Conceptualization, Data curation, Formal analysis, Investigation, Methodology, Writing – original draft. **Begum Gulsoy:** Data curation, Validation, Methodology, Investigation. **Jonathan E.H. Sansom:** Conceptualization, Validation, Methodology, Investigation. **James Marco:** Conceptualization, Methodology, Resources, Writing – review & editing.

Declaration of Competing Interest

The authors declare that they have no known competing financial interests or personal relationships that could have appeared to influence the work reported in this paper.

Acknowledgements

This work was funded by EPSRC, Jaguar Land Rover Limited and WMG University of Warwick, under the Prosperity Partnership grant, R004927. The authors would like to thank Guillaume Remy and Mark Williams from the Metrology and Visualisation research group, WMG, University of Warwick for their work performing x-ray CT scans with the instrumented cells. The authors would also like to thank Ivana Hasa (WMG, University of Warwick) for contributing assistance and advice during the preliminary studies involving the thermistor arrays and chemical compatability testing.

References

[1] C. Brand, J. Anable, I. Ketsopoulou, J. Watson, Road to zero or road to nowhere? Disrupting transport and energy in a zero carbon world, Energy Policy 139 (2020), https://doi.org/10.1016/j.enpol.2020.111334. Apr.

[2] S. Küfeoğlu, D.K.K. Hong, Emissions performance of electric vehicles: a case study from the United Kingdom, Appl. Energy 260 (2020), 114241, https://doi.org/10.1016/j.apenergy.2019.114241. Feb.

[3] B. Nykvist, O. Olsson, The feasibility of heavy battery electric trucks, Joule 5 (4) (2021) 901–913, https://doi.org/10.1016/j.joule.2021.03.007. Apr.

[4] S. Tanvir, F. Un-Noor, K. Boriboonsomsin, and Z. Gao, "Feasibility of operating a heavy-duty battery electric truck fleet for drayage applications:," 10.1177/0361198120957325, vol. 2675, no. 1, pp. 258–268, Nov. 2020, doi: 10.1177/0361198120957325.

[5] M. Tariq, A.I. Maswood, C.J. Gajanayake, A.K. Gupta, Aircraft batteries: current trend towards more electric aircraft, IET Electr. Syst. Transp. 7 (2) (2017) 93–103, https://doi.org/10.1049/iet-est.2016.0019. Jun.

[6] A. Bauen, N. Bitossi, L. German, A. Harris, K. Leow, Sustainable aviation fuels status, challenges and prospects of drop-in liquid fuels, hydrogen and electrification in aviation, Johns. Matthey Technol. Rev. 64 (3) (2020) 263–278, https://doi.org/10.1595/205651320x15816756012040. Jul.

[7] K. Rommel, J. Sagebiel, Are consumer preferences for attributes of alternative vehicles sufficiently accounted for in current policies? Transp. Res. Interdiscip. Perspect. 10 (2021), 100385 https://doi.org/10.1016/J.TRIP.2021.100385. Jun.

[8] T. Cai, P. Valecha, V. Tran, B. Engle, A. Stefanopoulou, J. Siegel, Detection of Li-ion battery failure and venting with carbon dioxide sensors, eTransportation 7 (2021), 100100, https://doi.org/10.1016/j.etran.2020.100100. Feb.

[9] W. Huang, X. Feng, X. Han, W. Zhang, F. Jiang, Questions and answers relating to lithium-ion battery safety issues, Cell Rep. Phys. Sci. 2 (1) (2021), 100285, https://doi.org/10.1016/J.XCRP.2020.100285. Jan.

[10] A. Weinkopf, B. Scholz, F. Mayr, C. Hochmuth, Crash tests with high-voltage vehicles, ATZelectronics Worldw. 16 (5) (2021) 16–22, https://doi.org/10.1007/S38314-021-0618-7, 2021 165May.

[11] T. Muneer, R. Milligan, I. Smith, A. Doyle, M. Pozuelo, M. Knez, Energetic, environmental and economic performance of electric vehicles: experimental evaluation, Transp. Res. Part D Transp. Environ. 35 (2015) 40–61, https://doi.org/10.1016/j.trd.2014.11.015. Mar.

[12] T. Grandjean, A. Barai, E. Hosseinzadeh, Y. Guo, A. McGordon, J. Marco, Large format lithium ion pouch cell full thermal characterisation for improved electric vehicle thermal management, J. Power Sources 359 (2017) 215–225, https://doi.org/10.1016/j.jpowsour.2017.05.016.

[13] X. Lin, H.E. Perez, J.B. Siegel, A.G. Stefanopoulou, Robust estimation of battery system temperature distribution under sparse sensing and uncertainty, IEEE Trans. Control Syst. Technol. (2019) 1–13, https://doi.org/10.1109/tcst.2019.2892019. Jan.

[14] R.R. Richardson, S. Zhao, D.A. Howey, On-board monitoring of 2-D spatially-resolved temperatures in cylindrical lithium-ion batteries: part II. State estimation via impedance-based temperature sensing, J. Power Sources 327 (2016) 726–735, https://doi.org/10.1016/j.jpowsour.2016.06.104. Sep.

[15] F.H. Gandoman, et al., Concept of reliability and safety assessment of lithium-ion batteries in electric vehicles: basics, progress, and challenges, Appl. Energy 251 (2019), 113343, https://doi.org/10.1016/j.apenergy.2019.113343. Oct.

[16] P. Sun, R. Bisschop, H. Niu, X. Huang, A review of battery fires in electric vehicles, Fire Technol. 56 (4) (2020) 1361–1410, https://doi.org/10.1007/S10694-019-00944-3, 2020 564Jan.

[17] G. Pandian, M. Pecht, E. Zio, M. Hodkiewicz, Data-driven reliability analysis of Boeing 787 Dreamliner, Chin. J. Aeronaut. (2020), https://doi.org/10.1016/j.cja.2020.02.003. Mar.

[18] C. Ozkurt, F. Camci, B. Esat, O. Toker, Cost benefit analysis of individual cell control in batteries for electric vehicles, in: Proceedings of the IEEE International Symposium on Industrial Electronics, 2014, pp. 1800–1804, https://doi.org/10.1109/ISIE.2014.6864888.

[19] A. Misra, Energy storage for electrified aircraft: the need for better batteries, fuel cells, and supercapacitors, IEEE Electrif. Mag. 6 (3) (2018) 54–61, https://doi.org/10.1109/MELE.2018.2849922. Sep.

[20] L.H. Saw, Y. Ye, A.A.O. Tay, Integration issues of lithium-ion battery into electric vehicles battery pack, J. Clean. Prod. 113 (2016) 1032–1045, https://doi.org/10.1016/j.jclepro.2015.11.011. Feb.

[21] P. Albertus, et al., Challenges for and pathways toward Li-metal-based all-solid-state batteries, ACS Energy Lett. 6 (4) (2021) 1399–1404, https://doi.org/10.1021/ACSENERGYLETT.1C00445. Apr.

[22] T.A. Vincent, J. Marco, Development of smart battery cell monitoring system and characterization on a small-module through in-vehicle power line communication, IEEE Access (2020), https://doi.org/10.1109/ACCESS.2020.3043657.

[23] T.A. Vincent, B. Gulsoy, J.E.H. Sansom, J. Marco, A smart cell monitoring system based on power line communication-optimization of instrumentation and acquisition for smart battery management, IEEE Access 9 (2021) 161773–161793, https://doi.org/10.1109/ACCESS.2021.3131382. Nov.

[24] M. Fleckenstein, O. Bohlen, M.A. Roscher, B. Bäker, Current density and state of charge inhomogeneities in Li-ion battery cells with LiFePO4 as cathode material due to temperature gradients, J. Power Sources 196 (10) (2011) 4769–4778, https://doi.org/10.1016/J.JPOWSOUR.2011.01.043. May.

[25] M.S. Wahl, L. Spitthoff, H.I. Muri, A. Jinasena, O.S. Burheim, J.J. Lamb, The importance of optical fibres for internal temperature sensing in lithium-ion batteries during operation, Energies 14 (12) (2021) 3617, https://doi.org/10.3390/EN14123617, 2021, Vol. 14, Page 3617Jun.

[26] R. Srinivasan, P.A. Demirev, B.G. Carkhuff, Rapid monitoring of impedance phase shifts in lithium-ion batteries for hazard prevention, J. Power Sources 405 (2018) 30–36, https://doi.org/10.1016/j.jpowsour.2018.10.014. Nov.

[27] J.B. Robinson, et al., Non-uniform temperature distribution in Li-ion batteries during discharge-a combined thermal imaging, X-ray micro-tomography and electrochemical impedance approach, J. Power Sources 252 (2014) 51–57, https://doi.org/10.1016/j.jpowsour.2013.11.059. Apr.

[28] Y. Lai, W. Wu, K. Chen, S. Wang, C. Xin, A compact and lightweight liquid-cooled thermal management solution for cylindrical lithium-ion power battery pack, Int. J. Heat Mass Transf. 144 (2019), 118581, https://doi.org/10.1016/j.ijheatmasstransfer.2019.118581. Dec.

[29] Q. Zhang, et al., Factors influencing the economics of public charging infrastructures for EV-a review, Renew. Sustain. Energy Rev. 94 (2018) 500–509, https://doi.org/10.1016/j.rser.2018.06.022. Oct.

[30] A. Kwade, W. Haselrieder, R. Leithoff, A. Modlinger, F. Dietrich, K. Droeder, Current status and challenges for automotive battery production technologies, Nat. Energy 3 (4) (2018) 290–300, https://doi.org/10.1038/s41560-018-0130-3. Apr.

[31] P.V. Chombo, Y. Laoonual, A review of safety strategies of a Li-ion battery, J. Power Sources 478 (2020), 228649, https://doi.org/10.1016/j.jpowsour.2020.228649. Dec.

[32] D. Worwood, R. Algoo, R.J. McGlen, J. Marco, D. Greenwood, A study into different cell-level cooling strategies for cylindrical lithium-ion cells in automotive applications, Int. J. Powertrains 7 (1–3) (2018) 199–226, https://doi.org/10.1504/IJPT.2018.090381.

[33] J.B. Robinson, et al., Non-uniform temperature distribution in Li-ion batteries during discharge combined thermal imaging, X-ray micro-tomography & electrochemical impedance approach, J. Power Sources 252 (2014) 51–57, https://doi.org/10.1016/j.jpowsour.2013.11.059. Apr.

[34] R. Carter, et al., Directionality of thermal gradients in lithium-ion batteries dictates diverging degradation modes, Cell Rep. Phys. Sci. 2 (3) (2021), 100351, https://doi.org/10.1016/J.XCRP.2021.100351. Mar.

[35] G.M. Cavalheiro, T. Iriyama, G.J. Nelson, S. Huang, G. Zhang, Effects of nonuniform temperature distribution on degradation of lithium-ion batteries, J. Electrochem. Energy Convers. Storage 17 (2) (2020), https://doi.org/10.1115/1.4045205. May.

[36] E. Hosseinzadeh, et al., Quantifying cell-to-cell variations of a parallel battery module for different pack configurations, Appl. Energy 282 (2021), 115859, https://doi.org/10.1016/j.apenergy.2020.115859. Jan.

[37] E. Maiser, Battery packaging-technology review, AIP Conf. Proc. 1597 (1) (2015) 204, https://doi.org/10.1063/1.4878489. Feb.

[38] G. Zhang, L. Cao, S. Ge, C.Y. Wang, C.E. Shaffer, C.D. Rahn, *In situ* measurement of radial temperature distributions in cylindrical Li-ion cells, J. Electrochem. Soc. 161 (10) (2014) A1499–A1507, https://doi.org/10.1149/2.0051410jes. Jul.

[39] L. Yang, et al., Internal field study of 21700 battery based on long-life embedded wireless temperature sensor, Acta Mech. Sin. 1 (2021) 1–7, https://doi.org/10.1007/S10409-021-01103-0, 2021Jun.

[40] J. Fleming, T. Amietszajew, J. Charmet, A.J. Roberts, D. Greenwood, R. Bhagat, The design and impact of *in-situ* and operando thermal sensing for smart energy storage, J. Energy Storage 22 (2019) 36–43, https://doi.org/10.1016/j.est.2019.01.026. October 2018.

[41] J. Fleming, T. Amietszajew, E. McTurk, D. Greenwood, R. Bhagat, Development and evaluation of *in-situ* instrumentation for cylindrical Li-ion cells using fibre optic sensors, HardwareX 3 (2018) 100–109, https://doi.org/10.1016/j.ohx.2018.04.001.

[42] S. Novais, et al., Internal and external temperature monitoring of a Li-ion battery with fiber bragg grating sensors, Sensors 16 (9) (2016) 1394, https://doi.org/10.3390/s16091394. Aug.

[43] Z. Wei, J. Zhao, H. He, G. Ding, H. Cui, L. Liu, Future smart battery and management: advanced sensing from external to embedded multi-dimensional measurement, J. Power Sources 489 (2021), 229462, https://doi.org/10.1016/j.jpowsour.2021.229462. Mar.

[44] S. Zhu, et al., A novel embedded method for *in-situ* measuring internal multi-point temperatures of lithium ion batteries, J. Power Sources 456 (2020), 227981, https://doi.org/10.1016/j.jpowsour.2020.227981. Apr.

[45] A. Fortier, M. Tsao, N. Williard, Y. Xing, M. Pecht, Preliminary study on integration of fiber optic bragg grating sensors in Li-ion batteries and *in situ* strain and temperature monitoring of battery cells, Energies 10 (7) (2017) 838, https://doi.org/10.3390/en10070838. Jun.

[46] R.R. Richardson, P.T. Ireland, D.A. Howey, Battery internal temperature estimation by combined impedance and surface temperature measurement, J. Power Sources 265 (2014) 254–261, https://doi.org/10.1016/j.jpowsour.2014.04.129. Nov.

[47] O.J. Curnick, J.E.H. Sansom, J. Harper, M. Tsiamtsouri, R. Bhagat, D. Greenwood, Rapid State-of-Health (SoH) determination and second-life grading of aged automotive battery modules via electrochemical impedance spectroscopy (EIS), ECS Meet. Abstr. MA2019-02 (1) (2019) 53, https://doi.org/10.1149/MA2019-02/1/53. Sep.

[48] E. Din, C. Schaef, K. Moffat, J.T. Stauth, A scalable active battery management system with embedded real-time electrochemical impedance spectroscopy, IEEE Trans. Power Electron. 32 (7) (2017) 5688–5698, https://doi.org/10.1109/TPEL.2016.2607519. Jul.

[49] P. Haussmann, J. Melbert, Sensorless individual cell temperature measurement by means of impedance spectroscopy using standard battery management systems of electric vehicles, SAE Tech. Pap. 2020-April (2020), https://doi.org/10.4271/2020-01-0863 no. April, Apr.

[50] A. De Angelis, R. Ramilli, M. Crescentini, A. Moschitta, P. Carbone, P.A. Traverso, *In-situ* electrochemical impedance spectroscopy of battery cells by means of binary

sequences, Conf. Rec., in: Proceedings of the IEEE Instrumentation and Measurement Technology Conference 2021-May, 2021 https://doi.org/10.1109/I2MTC50364.2021.9459998. May
[51] M. Ströbel, J. Pross-Brakhage, M. Kopp, K.P. Birke, Impedance based temperature estimation of lithium ion cells using artificial neural networks, Batteries 7 (4) (2021) 85, https://doi.org/10.3390/BATTERIES7040085, 2021, Vol. 7, Page 85Dec.
[52] N. Williard, W. He, C. Hendricks, M. Pecht, Lessons learned from the 787 dreamliner issue on lithium-ion battery reliability, Energies 6 (9) (2013) 4682–4695, https://doi.org/10.3390/en6094682.
[53] Y. Yu, et al., Distributed thermal monitoring of lithium ion batteries with optical fibre sensors, J. Energy Storage 39 (2021), 102560, https://doi.org/10.1016/j.est.2021.102560. Jul.
[54] E. Vergori, Y. Yu, Monitoring of Li-ion cells with distributed fibre optic sensors, Proced. Struct. Integr. 24 (2019) 233–239, https://doi.org/10.1016/j.prostr.2020.02.020.
[55] S.A. Mathew, R. Prakash, P.C. John, A smart wireless battery monitoring system for electric vehicles, in: Proceedings of the International Conference on Intelligent Systems Design and Applications, ISDA, 2012, pp. 189–193, https://doi.org/10.1109/ISDA.2012.6416535.
[56] L. Kang, et al., A flexible resistive temperature detector (RTD) based on *in-situ* growth of patterned Ag film on polyimide without lithography, Microelectron. Eng. 216 (2019), 111052, https://doi.org/10.1016/j.mee.2019.111052. Aug.
[57] C.Y. Lee, et al., Integrated microsensor for real-time microscopic monitoring of local temperature, voltage and current inside lithium ion battery, Sens. Actuators A Phys. 253 (2017) 59–68, https://doi.org/10.1016/j.sna.2016.10.011. Jan.
[58] N. Martiny, T. Mühlbauer, S. Steinhorst, M. Lukasiewycz, A. Jossen, Digital data transmission system with capacitive coupling for *in-situ* temperature sensing in lithium ion cells, J. Energy Storage 4 (2015) 128–134, https://doi.org/10.1016/J.EST.2015.10.001. Dec.
[59] D. Alonso, O. Opalko, K. Dostert, Parametrization of automotive lithium-ion batteries and its influence on the wireless in-battery channel, in: Proceedings of the 10th European Conference on Antennas and Propagation, EuCAP 2016, 2016, https://doi.org/10.1109/EuCAP.2016.7481269.
[60] Z. Sheng, D. Tian, V.C.M. Leung, G. Bansal, Delay analysis and time-critical protocol design for in-vehicle power line communication systems, IEEE Trans. Veh. Technol. 67 (1) (2018) 3–16, https://doi.org/10.1109/TVT.2017.2770182. Jan.
[61] J. Jousse, N. Ginot, C. Batard, E. Lemaire, Power line communication management of battery energy storage in a small-scale autonomous photovoltaic system, IEEE Trans. Smart Grid 8 (5) (2017) 2129–2137, https://doi.org/10.1109/TSG.2016.2517129. Sep.
[62] V. Lorentz, M. Wenger, M. Giegerich, S. Zeltner, M. März, L. Frey, Smart battery cell monitoring with contactless data transmission. Advanced Microsystems for Automotive Applications 2012: Smart Systems For Safe, Sustainable and Networked Vehicles, Springer, Berlin, Heidelberg, 2012, pp. 15–26.
[63] S. Bacquet, M. Maman, Radio frequency communications for smart cells in battery pack for electric vehicle, in: Proceedings of the IEEE International Electric Vehicle Conference, IEVC 2014, 2015, https://doi.org/10.1109/IEVC.2014.7056120.
[64] T. Bruen, J. Marco, Modelling and experimental evaluation of parallel connected lithium ion cells for an electric vehicle battery system, J. Power Sources 310 (2016) 91–101, https://doi.org/10.1016/j.jpowsour.2016.01.001. Apr.
[65] L. Somerville, S. Ferrari, M.J. Lain, A. McGordon, P. Jennings, R. Bhagat, An *in-situ* reference electrode insertion method for commercial 18650-type cells, Batteries 4 (2) (2018), https://doi.org/10.3390/batteries4020018. Jun.
[66] Allegro MicroSystems, "ACS37612 standalone current sensor," 2020. [Accessed: 03-Aug-2021]. Available: https://www.allegromicro.com/en/products/sense/current-sensor-ics/sip-package-zero-to-thousand-amp-sensor-ics/acs37612.
[67] J.R. Belt, D.M. Bernardi, V. Utgikar, Development and Use of a lithium-metal reference electrode in aging studies of lithium-ion batteries, J. Electrochem. Soc. 161 (6) (2014), https://doi.org/10.1149/2.062406jes.
[68] C. Xu, et al., Internal temperature detection of thermal runaway in lithium-ion cells tested by extended-volume accelerating rate calorimetry, J. Energy Storage 31 (2020), 101670, https://doi.org/10.1016/J.EST.2020.101670. Oct.
[69] Murata Manufacturing Co. Ltd., NCP03WF104F05RL|NTC for Temperature Sensor, Murata Temp. Sens. (2021) [Online]. Available: https://www.murata.com/en-eu/products/productdetail?partno=NCP03WF104F05RL [Accessed: 03-Aug-2021].
[70] A. Barai, K. Uddin, W.D. Widanage, A. McGordon, P. Jennings, A study of the influence of measurement timescale on internal resistance characterisation methodologies for lithium-ion cells, Sci. Rep. 8 (1) (2018) 1–13, https://doi.org/10.1038/s41598-017-18424-5, 2017 81Jan.
[71] M.F. Niri, T.M.N. Bui, T.Q. Dinh, E. Hosseinzadeh, T.F. Yu, J. Marco, Remaining energy estimation for lithium-ion batteries via Gaussian mixture and Markov models for future load prediction, J. Energy Storage 28 (2020), 101271, https://doi.org/10.1016/j.est.2020.101271. Apr.
[72] T.F. Landinger, G. Schwarzberger, G. Hofer, M. Rose, A. Jossen, Power line communications for automotive high voltage battery systems: channel modeling and coexistence study with battery monitoring, Energies 14 (7) (2021) 1851, https://doi.org/10.3390/en14071851. Mar.
[73] M.S. Saleem, Development of PLC based communication architecture for battery management system, in: Proceedings of the IEEE Vehicular Technology Conference 2020-May, 2020, https://doi.org/10.1109/VTC2020-Spring48590.2020.9128451.